Structural and metal-insulator transitions in rhenium-based double perovskites via orbital ordering

Alex Taekyung Lee and Chris A. Marianetti

Phys. Rev. B **97**, 045102 — Published 3 January 2018

DOI: 10.1103/PhysRevB.97.045102

Structural and metal-insulator transitions in rhenium based double perovskites via orbital ordering

Alex Taekyung Lee and Chris A. Marianetti
Department of Applied Physics and Applied Mathematics, Columbia University, New York, New York 10027, USA

Re-based double perovskites (DPs) have garnered substantial attention due to their high Curie temperatures (T_C) and display of complex interplay of structural and metal-insulator transitions (MIT). Here we systematically study the ground state electronic and structural properties for a family of Re-based DPs $A_2B\mathrm{ReO}_6$ (A=Sr, Ca and B=Cr, Fe), which are related by a common low energy Hamiltonian, using density functional theory + U calculations. We show that the on-site interaction U of Re induces orbital ordering (denoted C-OO), with each Re site having an occupied d_{xy} orbital and a C-type alternation among d_{xz}/d_{yz}, resulting in an insulating state consistent with experimentally determined insulators $\mathrm{Sr_2CrReO_6}$, $\mathrm{Ca_2CrReO_6}$, and $\mathrm{Ca_2FeReO_6}$. The threshold value of U_{Re} for orbital ordering is reduced by inducing E_g octahedral distortions of the same C-type wavelength (denoted C-OD), which serves as a structural signature of the orbital ordering; octahedral tilting also reduces the threshold. The C-OO, and the concomitant C-OD, are a spontaneously broken symmetry for the Sr based materials (i.e. $a^0a^0c^-$ tilt pattern), while not for the Ca based systems (i.e. $a^-a^-b^+$ tilt pattern). Spin-orbit coupling does not qualitatively change the physics of the C-OO/C-OD, but can induce relevant quantitative changes. We prove that a single set of $U_{\mathrm{Cr}}, U_{\mathrm{Fe}}, U_{\mathrm{Re}}$ capture the experimentally observed metallic state in $\mathrm{Sr_2FeReO_6}$ and insulating states in other three systems. We predict that the C-OO is the origin of the insulating state in $\mathrm{Sr_2CrReO_6}$, and that the concomitant C-OD may be experimentally observed at sufficiently low temperatures (i.e. space group $P4_2/m$) in pure samples. Additionally, given our prescribed values of U, we show that the C-OO induced insulating state in $\mathrm{Ca_2CrReO_6}$ will survive even if the C-OD amplitude is suppressed (e.g. due to thermal fluctuations). The role of the C-OO/C-OD in the discontinuous, temperature driven MIT in $\mathrm{Ca_2FeReO_6}$ is discussed.

PACS numbers: 71.30.+h, 75.70.Cn, 75.47.Lx, 75.25.Dk, 71.15.Mb

I. Introduction

A. General Background

There is a huge phase space of possibilities for perovskite based transition metal oxides with more than one type of transition metal which nominally bears d electrons, and experimental efforts are continuing to expand in this direction; including chemical synthesis[1–5] and layer-by-layer growth by pulsed laser deposition[4,6,7]. Given that many of these materials will exhibit strongly correlated electron behavior, it will be critical to have appropriate first-principles based approaches which can be applied to this vast phase space in order to guide experimental efforts; allowing for the development of novel, functional materials. Nearly two decades ago, room-temperature ferrimagnetism (sometimes loosely referred to as ferromagnetism) was discovered in the double-perovskite (DP) transition metal oxides (TMO) $\mathrm{Sr_2FeMoO_6}$[8], attracting much attention to DP TMO's due to their rich physics and potential for spintronic applications[4]. Recent first-principles efforts have shown promise in identifying new, novel materials in this phase space[9–12].

Among the various double perovskites, Re-based DPs are a particularly intriguing class; and the small set $A_2B\mathrm{ReO}_6$ (A=Sr, Ca and B=Cr, Fe) already contains a wealth of interesting physics and impressive metrics. Moreover, this particular set of Re-based DPs materials forms a sort of family which descends from the same low energy Hamiltonian of Re dominated orbitals, despite the fact that Cr and Fe have different numbers of electrons; and this can be deduced from nominal charge counting along with some amount of post facto knowledge (see Section III A for a more detailed explanation). Given that Sr and Ca are isovalent (i.e. nominally 2+), these two cations serve as binary parameter to modify the degree and type of octahedral tilting, changing the bandwidth of the system. Switching between Cr and Fe changes the valence by two electrons and alters the B site energy. However, Cr and Fe are totally analogous in the sense that both yield a filled spin shell given a predominant octahedral crystal field and a high spin configuration (i.e. $t^3_{2g,\uparrow}$ and $t^3_{2g,\uparrow}e^2_{g,\uparrow}$, respectively).

Experiment dictates that the resulting four permutations of $A_2B\mathrm{ReO}_6$ yield both metallic and insulating ground states, insulator to metal transitions as a function of temperature (for reasonable temperature scales), structural transitions as a function of temperature, and in some cases very high ferrimagnetic to paramagnetic transition temperatures. Moreover, this Re-based family of DP contains unexplained phenomena, such as the discontinuous, isostructural phase transition in $\mathrm{Ca_2FeReO_6}$. Therefore, there are a variety of phenomenological, qualitative, and quantitative challenges which need to be addressed in this family.

Given that all of these compounds are strongly mag-

netically ordered at low temperatures, it is reasonable to expect that DFT+U might provide an overarching, qualitative view of the physics; perhaps even quantitative. In this work, we use DFT+U calculations to investigate the electronic and structural aspects of $A_2B\mathrm{ReO}_6$ (A=Sr, Ca, and B=Cr, Fe), systematically accounting for the effects of octahedral distortions and rotations; in addition to carefully exploring the effect of the Hubbard U for both the B sites and Re. We show that a single set of $U_{\mathrm{Re}}, U_{\mathrm{Fe}}, U_{\mathrm{Cr}}$ can obtain qualitative agreement with known experiments of all four compounds. Particular attention is payed to isolating the effects of the Hubbard U by additionally considering cubic reference structures in the absence of any octahedral distortions or tilting. Finally, we explore the effect of spin-orbit coupling, demonstrating that it can perturb the C-OO and the resulting C-OD, but the qualitative trends hold.

The rest of the paper is organized as follows. Sections I B and I C address the previous literature of the Re-based double perovskites and orbital ordering physics in other perovskites, respectively. Section II details the computational methods and provides a brief discussion on the value of U, while a detailed analysis of the optimal U values is given in Section III D. Section III A provides a minimal analysis of the various physical mechanisms at play in this family of materials, highlighting the key findings in our paper; while detailed calculations which shape our conclusions can be found in Sections III B and III C. Section III E discusses future experiments which could test our predictions, and Section IV presents the summary of the paper.

B. Literature review of $A_2B\mathrm{ReO}_6$ (A=Sr, Ca and B=Cr,Fe)

Here we review the experimental literature, in addition to some of the theoretical literature, on our Re-based compounds of interest: $A_2B\mathrm{ReO}_6$ (A=Sr, Ca, and B=Cr, Fe). All four compounds form a perovskite structure with the Re/B atoms ordering in a $\boldsymbol{q}_{\mathrm{sc}} = \left(\frac{1}{2}, \frac{1}{2}, \frac{1}{2}\right)$ motif with respect to the primitive simple cubic perovskite lattice vectors (see Figure 2). All systems are ferrimagnetically ordered below room temperature with the Re and B atoms having opposite spins. We begin by presenting an experimental table of the crystal structures for the ground state and at temperatures above the structural transition; except for $\mathrm{Ca_2CrReO_6}$, which is not known to have a transition near room temperature (see Table I). Additionally, we tabulate the transition temperatures and the nature of the ground state (i.e. metal vs. insulator). We will also discuss other experimental viewpoints from the literature, some with dissenting views, that are not represented in this table.

Bulk $\mathrm{Sr_2FeReO_6}$ is tetragonal at 5K ($I4/m$, space group 87) as shown in Fig. 1(a), metallic (even in well ordered samples)[1,2,13,14], has $a^0a^0c^-$ octahedral tilting, and in-plane and out-of-plane ∠Fe-O-Re are 171.9 and 180°, respectively[2]. Upon increasing temperature, it undergoes a tetragonal-to-cubic phase transition at $T_t = 490K$ to space group 225 ($Fm\bar{3}m$), removing octahedral tilting.

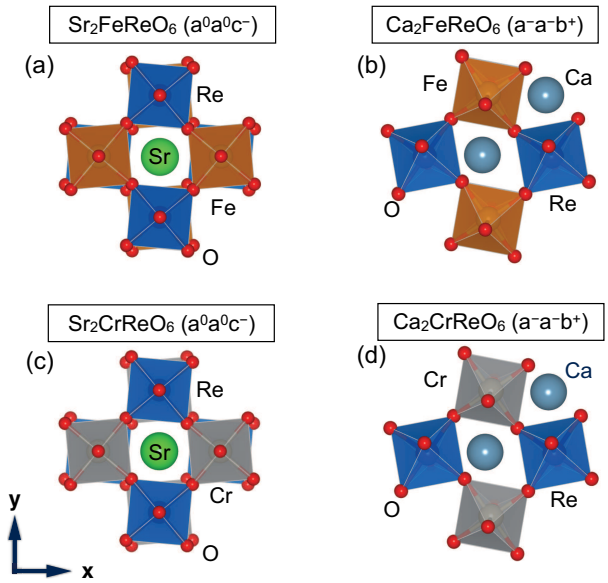

FIG. 1: Orthographic view of the crystal structures of (a) $\mathrm{Sr_2FeReO_6}$, (b) $\mathrm{Ca_2FeReO_6}$, (c) $\mathrm{Sr_2CrReO_6}$, and (d) $\mathrm{Ca_2CrReO_6}$. The octahedral tilt pattern in listed in each case.

$\mathrm{Ca_2FeReO_6}$ is monoclinic at 7K ($P2_1/n$, space group 14-2), and has $a^-a^-b^+$ octahedral tilting (see Fig. 1(b)). It is generally known as insulator at low temperature[1,14–16], though Fisher *et al.* suggested that it may be a bad metal[17]. With increasing temperature, $\mathrm{Ca_2FeReO_6}$ undergoes a concomitant structural and metal-insulator transition (MIT) at 140K[15,16]. Interestingly, the structures above and below the transition have the same space group symmetry, and octahedral tilting, but the structural parameters are slightly different[16]. Based on the experimental results, we infer that the predominant structural change at the phase transition is the enhancement and reorientation of a local axial octahedral distortion of the Re-O octahedron (i.e. linear combinations $A_{1g} + E_g$ octahedral modes, as defined from the cubic reference) which order in an C-type antiferro (i.e. $\boldsymbol{q}_{\mathrm{fcc}} = \left(0, \frac{1}{2}, \frac{1}{2}\right)$) manner with respect to the primitive face-centered cubic lattice vectors of the double perovskite (see Figure 2). We refer to this as a C-type octahedral distortion (C-OD) (see Table VI for projections onto the octahedral mode amplitudes).

The C-OD will be demonstrated to be a signature of orbital ordering of the Re electrons; which we will prove to be the common mechanism of the MIT in this entire family of materials. The C-OD is not a spontaneously broken symmetry in the space group of $\mathrm{Ca_2FeReO_6}$ (e.g. there is a small non-zero amplitude in the high temperature phase), and there are two symmetry inequivalent

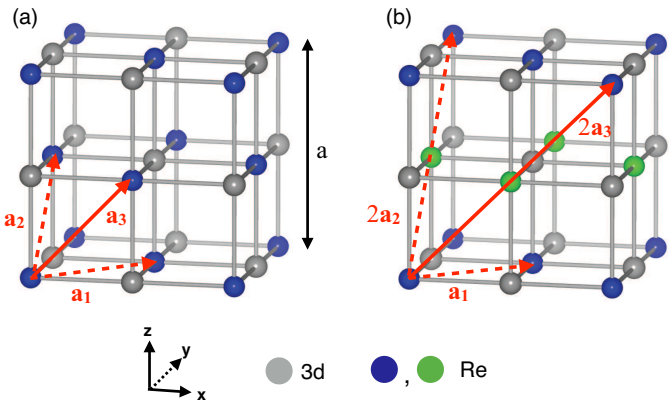

FIG. 2: Schematic of the Face-centered cubic (FCC) lattice of Re-based DP. Oxygen atoms are positioned at the midpoint between the Re and $3d$ site; though not pictured. Panel (a) defines the choice of primitive lattice vectors in cubic phase, corresponding to $\boldsymbol{a_1} = a/2(\hat{\imath} + \hat{\jmath})$, $\boldsymbol{a_2} = a/2(\hat{\jmath} + \hat{k})$, $\boldsymbol{a_3} = a/2(\hat{\imath} + \hat{k})$. Panel (b) shows the $\boldsymbol{q}_{\rm fcc} = (0, 1/2, 1/2)$ phase modulation of the Re atoms (i.e. green/blue color), along with the choice of supercell lattice vectors which accommodate this motif.

variants (i.e. C-OD$^+$ and C-OD$^-$, see Fig. 11) which represent the low and high temperature structures, respectively. Incidentally, the C-OD is a spontaneously broken symmetry in the Sr-based crystals (due to the $a^0a^0c^-$ tilt pattern), whereby C-OD$^+$ and C-OD$^-$ are identical by symmetry.

In order to clearly characterize the C-OD, the bond lengths of the Re-O octahedron from the experimental structures are summarized in Fig. 10. Above the structural transition, the Re-O bonds are split into three sets of two equal bond lengths (where the equal bonds arise from the inversion symmetry at the Re site), but two of the three sets are very similar. Specifically, at T=300K $d_{\text{Re1-O1}} = 1.959\mathring{A}$, $d_{\text{Re1-O2}} = 1.954\mathring{A}$, and $d_{\text{Re1-O3}} = 1.939\mathring{A}$, where Re1-O1 and Re1-O2 are approximately within the $a-b$ plane and Re1-O3 is approximately along the c-axis (see Fig. 5). In order to quantify relevant aspects of the octahedral distortions, we will define a parameter $d_{|x-y|} = |d_{\text{Re-O1}} - d_{\text{Re-O2}}|$, which is small in the high temperature phase (i.e. $d_{|x-y|} = 0.005\mathring{A}$ at T=300K); and $d_{|x-y|}$ is precisely the amplitude of the $E_g^{(0)}$ octahedral mode in the unrotated local coordinate system. For the symmetry equivalent Re within the unit cell (i.e. Re2), the nearly equivalent O1 and O2 bond lengths are swapped (i.e. $d_{|x-y|}$ is identical but the direction of the long/short bonds have reversed); while Re-O3 is identical.

Upon changing to the low temperature phase, there is a modest change whereby the Re-O3 bond length shifts up by $0.006\mathring{A}$ (i.e. equivalently in both Re), and a more dramatic change whereby the splitting between Re-O1 and Re-O2 becomes substantially larger (i.e. $d_{|x-y|} = 0.014\mathring{A}$). As in the high temperature structure, symmetry dictates that the direction of $d_{|x-y|}$ alternates between the two Re sites. The main difference is that $d_{|x-y|}$ acquires an appreciable value in the low temperature phase, and the C-OD switches between C-OD$^+$ and C-OD$^-$ (see Section III B 3 for a more detailed discussion).

Interestingly, Granado *et al.* suggested that there is phase separation between 10K and 650K, with all three phases being monoclinic[18]. More specifically, the most abundant phases are found to be the M1 and M2 phases, with fraction of 55% and 45%, respectively, and the main differences between the two phases are the b-lattice parameter and angle β. Similarly, Westerburg *et al.* also observed two different phases below 300K[19]. We note that the M1 and M2 phases in Granado *et al.*'s results[18] are similar to the low-T and high-T phases reported by Oikawa *et al.*, where the separation was not detected[16]. M1, which has the largest portion at low temperature, has a b lattice parameter which is ∼0.015Å smaller and a β which is ∼0.1° larger than those of the M2 phase, which constitutes ∼90% of the high T phase[18]. Similarly, at 140K, the low-T phase has smaller b and larger β than the high-T phase in Oikawa *et al.*'s report[16].

Having clarified the nature of the experimentally measured structural distortions in Ca_2FeReO_6, we return to the issue of the MIT as addressed in the literature. Since there are nominally only Re t_{2g} states near the Fermi level, the MIT is a gapping of these states. Oikawa *et al.* suggested that the d_{xy}+d_{yz} and d_{xy}+d_{zx} orbitals are randomly arranged at Re sites in the metallic phase, whereas the d_{yz}+d_{zx} orbitals are preferentially occupied in the insulating phase; and the splitting between d_{yz}+d_{zx} and d_{xy} orbitals produce the energy gap[16]. Previous local spin density functional theory (LSDA) studies showed that Ca_2FeReO_6 is metallic without considering on-site Coulomb repulsion U term for Re ($U_{\rm Re}$)[20,21] and a gap is opened with the large value U=3−4 eV[15,22].

Gong *et al.* concluded that the Re t_{2g} states order into a d_{xy}+d_{zx} configuration using the modified Becke-Johnson (mBJ) exchange-correlation potential, and showed that Ca_2FeReO_6 is insulating; though this study did not explicitly identify the C-type orbital ordering that drives this insulating state. A noteworthy approximation made in their work is that the atomic coordinates are relaxed within GGA, where $d_{|x-y|}$ is only 0.004Å, which is far smaller than low temperature experimental value in the insulating state. The importance of this amplified C-OD amplitude will be clearly demonstrated within our work.

Antonov *et al.*[23] reported the electronic structure of Ca_2FeReO_6 using LSDA+U+spin-orbit-coupling calculations. Using structures obtained from experiment at different temperatures, which encompasses the discontinuous phase transition at T=140K[16], they showed that spin and orbital moments also have abrupt changes across the transition, while both change linearly with structures from temperatures below and above the MIT[23].

TABLE I: Space group (sym), amplitude of the $E_g^{(0)}$ octahedral mode ($d_{|x-y|}$, in units of $\AA$) for Re, and metallic/insulating (M/I) nature for both low and high temperatures of Re-based DPs. Magnetic transition temperatures (T_C) and structural phase transition temperature (T_t) are also tabulated. Question marks indicate unknown or uncertain data.

Materials	T_C	T_t	T	sym	$d_{\|x-y\|}$	M/I
Sr_2FeReO_6	420K[a]	490K[a]	5K	$I4/m$[a]	0[a]	M[a]
			500K	$Fm\bar{3}m$	0	M
Sr_2CrReO_6	620K[a]	260K[a]	2K	$I4/m$?[*]	?[*]	I[b]
			300K	$Fm\bar{3}m$[a]	0[a]	M[a,b]
Ca_2FeReO_6	540K[c]	140K[c]	7K	$P2_1/n$[c]	0.014[c]	I[c]
			300K	$P2_1/n$	0.005	M
Ca_2CrReO_6	360K[d]	?	4.2K	$P2_1/n$[d]	?	I[d]
			300K	$P2_1/n$	0.005[d]	I

[*] a recent experiment finds an insulating state, but the structural parameters have not been measured[3]
[a] ref.[2] [b] ref.[3] [c] ref.[16] [d] ref.[1]

Sr_2CrReO_6 has been determined to be tetragonal with an $a^0a^0c^-$ octahedral tilt pattern (i.e. space group $I4/m$, see Fig. 1(c))[1,2]. Teresa *et al.* reported a structural transition at $T = 260K$, going from $I4/m$ to $Fm\bar{3}m$ (with increasing temperature) whereby the octahedral tilts and the tetragonality are disordered. Alternatively, Kato *et al.* found that Sr_2CrReO_6 is still $I4/m$[1,24] at room temperature, implying that the transition temperature was even higher in these particular samples; while Winkler *et al.* found that it was cubic ($Fm\bar{3}m$) at room temperature[25]. This is likely a minor discrepancy given that the structure measured by Kato *et al.* at room temperature (300K) only has small deviations from $Fm\bar{3}m$: the in-plane Cr-O-Re angle in the tetragonal structure is 179.7°, close to 180°, and the lattice parameters are nearly cubic with $\sqrt{2}a$=7.817 and c=7.809 Å[1].

Recent experiments have found Sr_2CrReO_6 to be insulating at low temperatures, in contrast with earlier work which found metallic states. Specifically, Hauser *et al.* found that a Sr_2CrReO_6 film grown on STO, where the strain is less than 0.05%, is insulating at 2K with a 0.21eV energy gap[3]. Alternatively, numerous samples obtained from chemically synthesis were all found to be metallic[1,2,24,25], in addition to previous thin film samples[26]. It should be noted that Kato *et al.* emphasized that Sr_2CrReO_6 is a very bad metal, and lies at the vicinity of a Mott-insulating state[24]. Moreover, Hauser *et al.* suggested that oxygen vacancies are the reason why Sr_2CrReO_6 samples reported in previous studies were metallic[27,28]. Indeed, previously reported metallic Sr_2CrReO_6 samples have a large amount of defects, such as Cr/Re anti-site defect: 9%[29], 15%[30], 10−12%[2], and 23.3%[1]. However, there is not yet theoretical justification for why Sr_2CrReO_6 might be an insulator. Unfortunately, full structural parameters have not yet been extracted from the insulating film at low temperatures[3], which could reveal signatures of an orbitally ordered insulator which we predict in our analysis (see Section III B 2).

To our knowledge, there are only few experiments on Ca_2CrReO_6[1,24]; finding a monoclinic crystal structure (space group $P2_1/n$, see Fig. 1(d)) and an insulating ground state. The energy gap is not reported yet, though the reflectivity spectra and optical conductivity were measured[24]. Theoretically, the recent mBJ study of Gong *et al.* suggested that the energy gap is 0.38eV, much larger than that of Ca_2FeReO_6. The resistivity curve suggests that it is still insulating at room temperature, but the resistivity will have an error given the 12-13.7% of B-site disorder[1,24], similar to the case of Sr_2CrReO_6. In addition, structural parameters as a function of temperature have not yet been reported, which will be relevant to testing the predictions in our study.

In the existing literature, the effect of electronic correlation, orbital ordering, and octahedral distortions have not been sufficiently isolated to give a universal understanding of this family. Most importantly, the origin of the MIT and it's relation to orbital ordering and the concomitant C-OD have not been elucidated. Theory and computation will be critical to separating cause from effect.

C. Orbital ordering

Orbital ordering is a well known phenomena in transition metal oxides[31–33], and it can drive a material into an insulating ground state. Two main mechanisms which drive orbital ordering are the electron-lattice (e-l) coupling, with a very relevant scenario being the well known Jahn-Teller (JT) Effect, and electron-electron (e-e) interactions. Disentangling these two effects in a real system can be challenging, as both mechanisms result in orbital ordering and a concomitant lattice distortion; though the latter could be vanishingly small in the case of e-e driven orbital ordering. A complicating factor in both theory and experiment is that preexisting structural distortions (e.g. octahedral tilting) may preclude the orbital ordering from being a spontaneously broken symmetry; meaning that orbital ordering is always present and the only question is a matter of degree. In the event that the e-e interactions are driving the ordering, a further question is if orbital ordering is critical to realizing the insulating state (ie. Slater-like e-e driven orbital ordered insulator) or if Mott physics generates the insulating state (ie. the system remains insulating even if the orbitals are thermally disordered). This latter question can also be cumbersome to disentangle.

In the context of DFT+U calculations, the Hubbard U captures a very relevant portion of the e-e interactions which drive orbital-ordering; similar to the U in a model Hamiltonian which gives rise to superexchange[31]. The

TABLE II: Space group (sym), amplitude of the $E_g^{(0)}$ octahedral mode ($d_{|x-y|}$) for orbitally active transition metal, and metallic/insulating (M/I) nature for both low and high temperatures of various perovskites which have orbital ordering. Magnetic transition temperatures ($T_{\rm mag}$) are also tabulated, where $T_{\rm mag} = T_N$, except for $YTiO_3$, and Ba_2NaOsO_6, where $T_{\rm mag} = T_C$. Question marks indicate unknown or uncertain data.

Materials	$T_{\rm mag}$	T	sym	$d_{\|x-y\|}$ (Å)	M/I	ref
$LaMnO_3$	140K	300K	$Pbnm$	0.271[a]	I	34–38
		798K	$Pbnm$	0.047	M[b]	
$KCuF_3$	38K	300K	$I4/mcm$	0.372[c]	I	39–44
		900K	$I4/mcm$	0.453	I?	
$LaTiO_3$	146K	8K	$Pbnm$	0.021[d]	I	45–55
		293K	$Pbnm$	0.026	I	
$YTiO_3$	30K	2K	$Pbnm$	0.054[e]	I	50–64
		290K	$Pbnm$	0.051	I	
$LaVO_3$	143K	10K	$P2_1/n$	0.061[f]	I	65–72
		150K	$Pbnm$	0.013	I	
		295K	$Pbnm$	0.001	I	
YVO_3*	116K	5K	$Pbnm$	0.050[g]	I	69–80
		295K	$Pbnm$	0.014	I	
Ba_2NaOsO_6	7K	5K	$Fm\bar{3}m$	0[h]	I	81–89
		high T	$Fm\bar{3}m$	0	?	
Sr_2CeIrO_6	21K	2K	$P2_1/n$	0.008[i]	I	90,91
		300K	$P2_1/n$	0.043	I	

[a] ref.[34] [b] ref.[35] [c] ref.[39] [d] ref.[45] [e] ref.[56] [f] ref.[65] [g] ref.[73] [h] ref.[83] [i] ref.[90]

* YVO_3 is $P2_1/n$ between 77K and 200K.

e-l coupling is accounted for in the DFT portion of the calculation (assuming a local or semi-local approximation to the DFT functional). If experimentally deduced orbital ordering is accounted for at the level of DFT (ie. U=0), then e-l couplings are likely playing a dominant role; while if DFT does not predominantly capture the orbital ordering, then the e-e interactions are likely playing a dominant role. In this case of dominant e-e interactions, if a particular spatial ordering is a necessary condition to drive an insulating state within DFT+U (for a physical value of U), then the resulting insulating state could be labeled as Slater-like. If an insulating state is achieved for an arbitrary ordering of the orbitals, then the system would be considered Mott-like.

Classic examples of perovskites which display antiferro orbital ordering, and are insulators, include the $3d^4$ $LaMnO_3$[34–38] and the $3d^9$ $KCuF_3$[39–44] which have ordering of e_g electrons; the $3d^1$ (t_{2g}) materials $LaTiO_3$ and $YTiO_3$[45–64]; and the $3d^2$ (t_{2g}) perovskites $LaVO_3$ and YVO_3[65–80]. It is useful to make some empirical characterization of these classic examples to provide context for the orbital ordering we identify in this study (see Table II). All of these systems are insulators until relatively high temperatures.

All of the aforementioned examples have the $GdFeO_3$ tilt pattern ($a^-a^-b^+$) except $KCuF_3$, and thus there is only orbital degeneracy in $KCuF_3$ (assuming a reference state where the $E_g^{(1)}$ strain mode is zero). Therefore, antiferro orbital ordering could be a spontaneously broken symmetry for $KCuF_3$, while the other systems will always display some degree of orbital polarization and octahedral distortion. In all cases, the most relevant lattice distortion is an $E_g^{(0)}$ distortion, driven by both e-l and e-e interactions. The e-l coupling is generally much larger for scenarios involving e_g electrons as compared to t_{2g}.

DFT+U calculations can be helpful in disentangling the effects of e-e interactions and e-l coupling. In the aforementioned classic examples of orbital ordering involving e_g electrons, important contributions are realized from both e-e interactions and e-l coupling. In $LaMnO_3$, an antiferro $E_g^{(0)}$ Jahn-Teller distortion, and corresponding orbital ordering, is found even at the level of GGA (ie. $U_{\rm Mn}$=0): the e-l coupling is strong enough to recover 0.8 of the experimentally observed Jahn-Teller distortion[36]. However, a non-zero $U_{\rm Mn}$ is needed to properly capture the energy stabilization, insulating ground state, and full magnitude of the Jahn-Teller distorted, orbitally ordered state. In $KCuF_3$, pure GGA is sufficient to spontaneously break symmetry and obtain the antiferro $E_g^{(0)}$ Jahn-Teller distortion that is observed in experiment, though the stabilization energy is grossly underestimated and the distortion magnitude is too small[42]. Including the on-site U gives reasonable agreement with experiment (both within DFT+U and DFT+DMFT)[40–42]. Alternatively, if one remains in the cubic reference structure, preventing coupling with the lattice, an on-site U of 7eV can drive the orbitally ordered insulator with a corresponding transition temperature of roughly 350K[41]. Therefore, both mechanism can drive the same instability, but in isolation the on-site U recovers a larger component of the stabilization energy; though both ingredients are necessary to quantitatively describe experiment. In both $LaMnO_3$ and $KCuF_3$, e-e interactions and e-l coupling both play a direct, relevant role.

In the t_{2g}-based systems, the e-l coupling is expected to be smaller. DFT+U studies for $LaTiO_3$ show that at U=0, the system is metallic and has a very small $E_g^{(0)}$ distortion of $d_{|x-y|}$=0.004−0.005$\AA$[92,93]; in contrast to experiment which yields an insulator with $d_{|x-y|}$=0.021$\AA$. Increasing the e-e interactions to U=3.2eV/J=0.9eV[92], an insulator is obtained and $d_{|x-y|}$=0.018$\AA$, in much better agreement with experiment (see Table II). DFT will always have a small value of $d_{|x-y|}$ due to the broken symmetry caused by the octahedral tilting, and the e-l coupling within DFT provides no strong enhancement of this distortion. Applying the Hubbard U both orders the orbitals and induces an appreciable value of $d_{|x-y|}$. This concomitant $d_{|x-y|}$ distortion may increase the potency

of the Hubbard U, such as increasing the resulting band gap (See results of Re-based family in Section III). The vanadates behave in a similar fashion. DFT (ie. U=0) calculations for $LaVO_3$, for the low-temperature phase $P2_1/n$ (or alternatively, $P2_1/a$ or $P2_1/b$), showed that $LaVO_3$ is metallic and $d_{|x-y|}$=0.001-0.002$\AA$[93], in stark disagreement with experiment which shows insulating behavior and $d_{|x-y|}$=0.061$\AA$ (see Table II). Hybrid functional calculations, which are very similar in nature to DFT+U, recover the insulating state and a appreciable $d_{|x-y|}$ amplitude. In these t_{2g}-based systems, DFT gets $d_{|x-y|}$ wrong by a factor of approximately 4-5 and 30-60 for the titanates and the vanadates, respectively; a much more dramatic failure than in the e_g-based materials.

Within experiment, one cannot easily isolate different terms in the Hamiltonian, though it may be possible to thermally quench the lattice distortion and determine if the orbital polarization persists. If so, this would strongly indicate that *e-e* interaction are dominant in driving orbital ordering. Furthermore, experiment could possibly determine if the system remains gapped upon thermally disordering the orbitals. As mentioned above, octahedral tilting is often a higher energy scale which already breaks symmetry, and it will not be totally clear what the quenched value of the distortion and or the orbital polarization should be. Below we tabulate the amplitude of the $E_g^{(0)}$ distortion and the metallic/insulating nature at a low temperature (i.e. a temperature below the orbital ordering) and a high temperature (i.e. either above the orbital ordering or the highest temperature measured); the magnetic transition temperatures are also included.

Three scenarios can be identified. First, the $E_g^{(0)}$ distortion may be essentially unchanged as a function of temperature, or even enhanced, while the material remains insulating (i.e. $KCuF_3$, $LaTiO_3$, and $YTiO_3$). Second, the $E_g^{(0)}$ distortion may be largely quenched via temperature and the system concomitantly becomes metallic (i.e. $LaMnO_3$). Third, the $E_g^{(0)}$ distortion may be largely quenched and the system remains insulating (i.e. $LaVO_3$ and YVO_3). In the first two scenarios, little can be deduced without further analysis: the orbital ordering and structural distortion are either frozen in or are simultaneously washed out. For the vanadates, we learn that the lattice distortion is irrelevant for attaining the insulating state: *e-e* interactions drive the orbital ordering. Further analysis would be needed to know if the insulator is Slater-like or Mott-like.

The orbital ordering which we identify in the 3d-5d Re-based DP's of this study has a number of distinct circumstances as compared to these classic 3d single perovskites. First, in the Re-DP's the magnetic transition temperatures (T_{mag}) are a much larger energy scale (see Table I), which means that the spins are strongly ordered well before orbital physics comes into play; whereas the reverse is true in the single 3d perovskites. Another difference is that the electronic structure of the 3d-5d DPs are generally governed by 5d orbitals, which may have a non-trivial spin-orbit interaction[85]. While 5d orbitals are more delocalized than 3d orbitals, it should be kept in mind that that the rock salt ordering of the DP's results in relatively small effective Re bandwidths (see Section III A).

A well studied class of DP's where orbital ordering may be relevant is the $A_2BB'O_6$ double perovskites, where B has fully filled or empty d orbital and B' is a 5d transition metal. One well studied type of family is the B'=5d^1 Mott insulators, such as Ba_2BOsO_6 (B=Li, Na)[81–89] and Ba_2BMoO_6 (B=Y, Lu)[83] (see Table II). These materials have very weak magnetic exchange interactions (e.g. T_C of Ba_2NaOsO_6 is 6.8-8 K[81–83]), and exotic phases have been proposed such as quantum-spin-liquids, valence-bond solids, or spin-orbit dimer phases[85,86]. Xiang *et al.*[84] studied Ba_2NaOsO_6 using the first-principles calculations, and suggested that an insulating phase cannot be obtained within GGA+U up to $U-J$=0.5 Ryd: orbital ordering is not observed in their electronic band structure within GGA+U. They also show that Ba_2NaOsO_6 is insulating within GGA+U when including spin-orbit coupling (SOC) with $U-J$=0.2Ryd and the [111] magnetization axis. Gangopadhyay *et al.*[88,89] also proposed that SOC is essential to obtain a nonzero band gap, using hybrid functional + SOC calculations. Based on experiment, Erickson *et al.* proposed that Ba_2NaOsO_6 has orbital ordering with a non-zero wavevector, deduced in part from the small negative Weiss temperature from magnetic susceptibility measurements[81].

Another analogous example is the Ir-based double perovskite Sr_2CeIrO_6 (see Table II), where Ce has a filled shell and the Ir 5d nominally have 5 electrons (or one hole) in the $e_g^\pi + a_{1g}$ orbitals (i.e. descendants of t_{2g})[91], and this results in weak antiferromagnetic coupling (i.e. T_N=21K). Additionally, orbital ordering has been identified in this material, where the hole orders in the e_g^π shell among the d_{xz} and d_{yz} orbitals with an antiferro modulation. The orbital ordering is accompanied by a $E_g^{(0)}$ structural distortion, though the experimental temperature dependence is rather unusual. At 2K and 300K, $d_{|x-y|}$=0.008$\AA$ and $d_{|x-y|}$=0.043$\AA$, respectively (see Table II), showing a strong increase in amplitude with increasing temperature[90]; while $d_{|x-y|}$=0.049$\AA$ is obtained within GGA+U (U=4eV and J=1eV)[91]. The authors attribute the orbital ordering to the Jahn-Teller effect, though they demonstrate that $U_{\rm Ir}$ is a necessary condition for opening a band gap[91]. It should be noted that the wavevector of the antiferro orbital and structural ordering in this system is the same as what we identify in the Re-based family in the present work.

Re-based double perovskites are quiet distinct from the aforementioned double perovskites with empty or fully filled d shell on the B ion. Unlike these latter materials, Re-based DPs have nonzero magnetic spin for B (e.g., Cr has spin 3/2 and Fe has spin 5/2), and thus have a strong antiferromagnetic exchange interaction between B and B'; resulting in a T_C that is much higher than room temperature (e.g. T_C in Sr_2CrReO_6 is 620K, see Table I).

Therefore, the spin degrees of freedom are locked in until relatively high temperatures, creating an ideal testbed to probe orbital physics. The family of Re-based DP's evaluated in this study are ideally distributed in parameter space about the orbital ordering phase transition.

II. Computation Details

We used the projector augmented wave (PAW) method[94,95] in order to numerically solve the Kohn-Sham equations, as implemented in the VASP code[96]. The exchange-correlation functional was approximated using the revised version of the generalized gradient approximation (GGA) proposed by Perdew *et al.* (PBEsol)[97]. In all cases, the spin-dependent version of the exchange correlation functional is employed; both with and without spin-orbit coupling (SOC). A plane wave basis with a kinetic energy cutoff of 500 eV was employed. We used a Γ-centered **k**-point mesh of 9×9×7 (11×11×9 for density of states). Wigner-Seitz radii of 1.323, 1.164, and 1.434 Å were used for site projections on Cr, Fe and Re atoms, respectively, as implemented in the VASP-PAW projectors.

The GGA+U scheme within the rotationally invariant formalism and the fully localized limit double-counting formula[40] is used to study the effect of electron correlation. The electronic and structural properties critically depend on U_{Re}, and therefore we carefully explore a range of values. We also explore how the results depend on U_{Cr} and U_{Fe}, which play a secondary but relevant role in the physics of these materials. We do not employ an on-site exchange interaction J for any species, as this is already accounted for within the spin-dependent exchange-correlation potential[98,99].

A post facto analysis of our results demonstrate that a single set of values (which are reasonable as compared to naive expectations and previous work) can account for the electronic and crystal structure of this family (see Section III D), and it is useful to provide this information at the outset for clarity. In the absence of spin-orbit coupling, values of U_{Fe}=4 eV, U_{Cr}=2.5 eV, and U_{Re}=2 eV are found; including spin-orbit coupling requires U_{Re} to be slightly decreased to 1.9 eV in order to maintain the proper physics. In subsequent discussions, the units of U will always be in electron volts (eV), and this may be suppressed for brevity.

We used experimental lattice parameters throughout (see Table I), and the reference temperature is 300K unless otherwise specified. Atomic positions within the unit cell were relaxed until the residual forces were less than 0.01 eV/Å. In select cases we do relax the lattice parameters as well to ensure no qualitative changes occur, and indeed the changes are small and inconsequential in all cases tested.

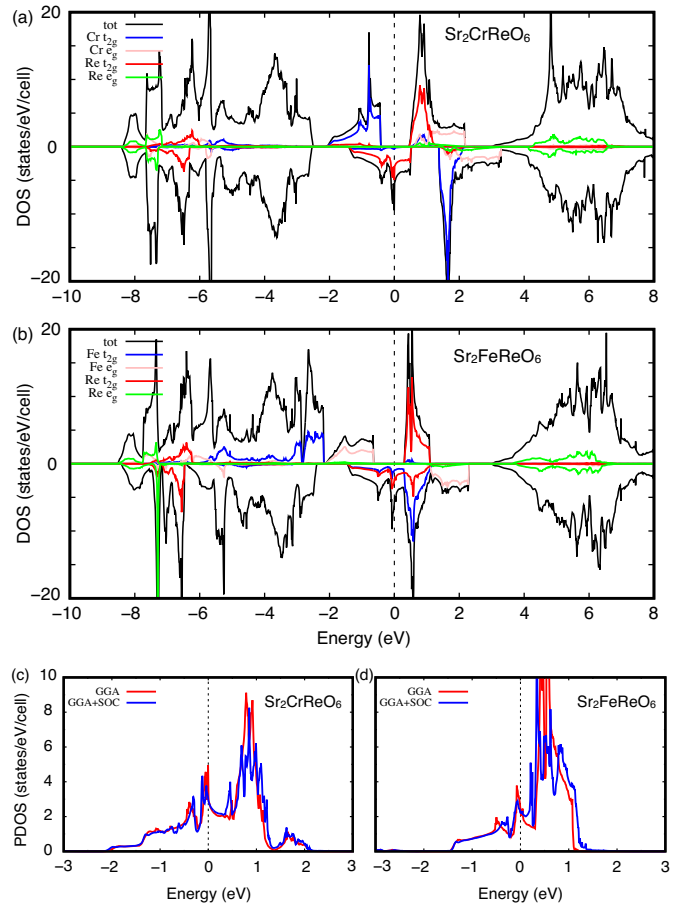

FIG. 3: (a),(b) Total and atom/orbital projected spin-resolved density of states (DOS) from DFT for (a) Sr_2CrReO_6 and (b) Sr_2FeReO_6. The majority spin are shown as a positive DOS while the minority are negative. Orbital projections are given for t_{2g} and e_g states for Re, Fe, and Cr. (c),(d) Illustrating the effect of spin-orbit coupling in the Re Projected density of states, comparing GGA (red solid line) and GGA+SOC (blue solid line) for (c) Sr_2CrReO_6 and (d) Sr_2FeReO_6. For GGA, majority and minority spins are summed for comparison. The Fermi energy is zero in all panels, and Fm$\bar{3}$m is used throughout.

III. Results and discussion

A. General Aspects of the Electronic Structure

We begin by discussing the nominal charge states of the transition metals, the basic energy scales, and the common mechanism of the metal-insulator transition in these compounds; which is a C-type antiferro orbital ordering. A perfect cubic structure ($Fm\bar{3}m$) is first considered, in the absence of SOC (which will be addressed at the end of this discussion). Given the Re double perovskite $A_2B\mathrm{ReO}_6$ (A=Sr,Ca, B=Fe,Cr), nominal charge counting dictates that the transition metal pair BRe must collectively donate 8 electrons to the oxygen (given that A_2

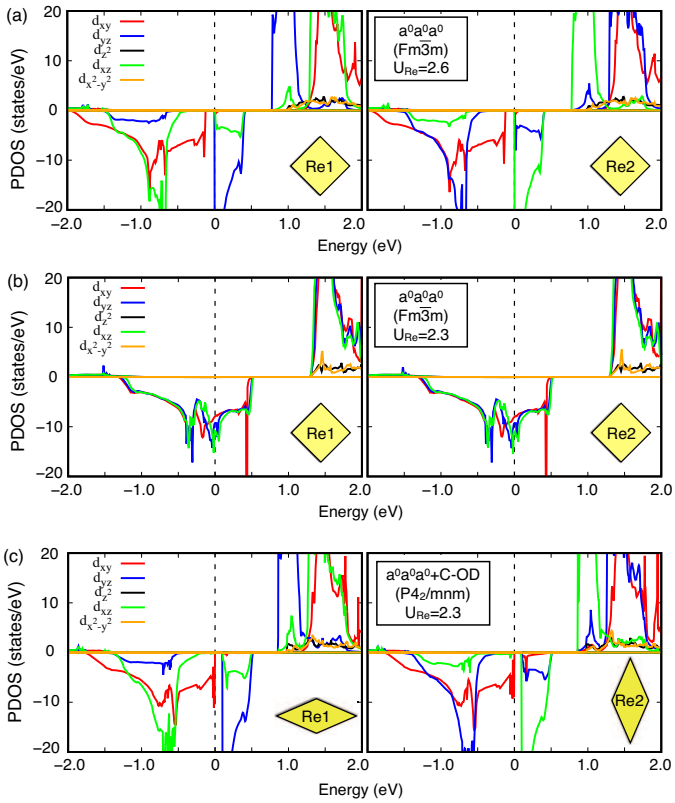

FIG. 4: Re projected density of states (PDOS) for Sr_2CrReO_6 within DFT+U. (a) $Fm\bar{3}m$ crystal structure and $U_{\rm Re}$=2.6, resulting in an orbitally ordered insulator. (b) $Fm\bar{3}m$ crystal structure and $U_{\rm Re}$=2.3, resulting in a metal. (c) $P4_2/mnm$ crystal structure (ie. $a^0a^0a^0$ tilt, with C-OD) and $U_{\rm Re}$=2.3, resulting in an orbitally ordered insulator. $U_{\rm Cr}$=0 in all cases.

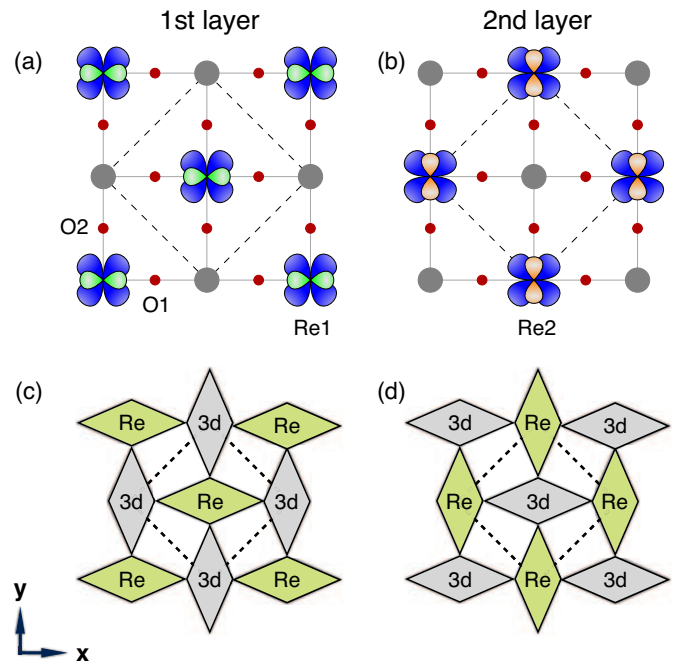

FIG. 5: Schematic diagrams of the C-type orbital ordering for the 1st and 2nd layer along the c-axis of the conventional cubic cell, shown in panels (a) and (b), respectively. Red dots correspond to oxygen atoms while grey dots correspond to B atoms (ie. Cr or Fe). The pictured t_{2g} orbitals are located on Re sites (d_{xy} is blue, d_{xz} is green, d_{yz} is orange). Panels (c) and (d) depict a schematic of the C-OD type structural distortion, whereby each local octahedron is distorted in a positive or negative $E_g^{(0)}$ distortion. Positive $E_g^{(0)}$ corresponds to the elongation along the y-direction and contraction along the x-direction (see Ref.[100] for formula). Dotted lines correspond to the unit cell.

donates 4 electrons), and it is energetically favorable (as shown below) to have Re^{5+} (d^2) and B^{3+} (Cr$\rightarrow d^3$ and Fe $\rightarrow d^5$) in a high spin configuration. The Re spin couples antiferromagnetically to the B spin via superexchange, yielding a ferrimagnetic state. Given that the nominally d^5 Fe has a half filled shell when fully polarized, and that the nominally filled d^3 Cr has a half-filled t_{2g}-based shell when fully polarized, none of these compounds would be expected to have Fe or Cr states at the Fermi energy when strongly polarized. Given that Re is in a d^2 configuration, group theory dictates that the system will be metallic with majority spin Re states present at the Fermi energy within band theory.

These naive expectations are clearly realized in DFT calculations (ie. U=0), as illustrated in Sr_2CrReO_6 and Sr_2FeReO_6 using the $Fm\bar{3}m$ structure (see Figure 3). It is useful to compare the Re states crossing the Fermi energy, which are substantially narrower for Sr_2CrReO_6 as compared to Sr_2FeReO_6. Relatedly, the Cr states hybridize less with and are further from the Re states as compared to the case of Fe. The net result is that the Cr based compounds will have a smaller effective Re bandwidth, and therefore stronger electronic correlations which result in a higher propensity to form an insulating state.

At the level of DFT+U, or any static theory for that matter, one can only obtain an insulator from the fully spin-polarized scenario outlined above via an additional spontaneously broken symmetry, which could be driven either via the on-site Re Coulomb repulsion $U_{\rm Re}$, structural distortions (which includes effects of electron-phonon coupling), or combinations thereof. As we will detail in the remainder of the paper, structural distortions alone (i.e. if $U_{\rm Re}$=0) cannot drive an insulating state in any of the four Re-based materials studied. Therefore, a non-zero $U_{\rm Re}$ is a *necessary condition* to drive the insulating state, but the minimum required value of $U_{\rm Re}$ will be influenced by the details of the structural distortions; in addition to the on-site U of the $3d$ transition metal and the SOC.

In order to illustrate the points of the preceding paragraph, we show that DFT+U calculations (with the only nonzero U being $U_{\rm Re}$=2.6) for Sr_2CrReO_6 with the nu-

clei frozen in the $Fm\bar{3}m$ structure results in a spontaneously broken symmetry of the electrons where the Re orbitals order and result in an insulating state (see Figure 4, panel a). We investigated ordered states consistent with $\boldsymbol{q}_{\rm fcc} = (0,0,0)$, $\boldsymbol{q}_{\rm fcc} = (0,0,\frac{1}{2})$, $\boldsymbol{q}_{\rm fcc} = (0,\frac{1}{2},\frac{1}{2})$, and $\boldsymbol{q}_{\rm fcc} = (\frac{1}{2},\frac{1}{2},\frac{1}{2})$ (where q is a fractional coordinate of the reciprocal lattice vectors constructed from the primitive FCC DP lattice vectors; see Fig. 2); resulting in a ground state of $\boldsymbol{q}_{\rm fcc} = (0,\frac{1}{2},\frac{1}{2})$ (ie. C-type ordering). Specifically, a Re d_{xy} orbital is occupied on every site and there is a C-type alternation between d_{xz} and d_{yz} (see schematic in Figure 5, panels a and b). This C-type antiferro orbital ordering (denoted as C-OO) is generic among this $A_2B\mathrm{ReO}_6$ family. We will demonstrate that other orderings are possible and even favorable under certain conditions. For example, for small values of $U_{\rm Re}$, the orbitals order in a ferro fashion (denoted F-OO), whereby the d_{xy} and either the d_{xz} or d_{yz} is occupied at every Re site. For intermediate values of $U_{\rm Re}$, a ferri version of the C-OO ordering (denoted FI-OO) is found, though it is destroyed by octahedral tilts. These detailed scenarios are explored in Section III B.

We now turn to the importance of structural distortions, such as the E_g octahedral distortions which are induced by the orbital ordering. We first remain in the $Fm\bar{3}m$ structure and lower the value of $U_{\rm Re}$ to 2.3eV, demonstrating that the orbital ordering is destroyed and the gap is closed (see Figure 4, panel b). Subsequently, we allow any internal relaxations of the ions consistent with $\boldsymbol{q}_{\rm fcc} = (0,0,0)$ or $\boldsymbol{q}_{\rm fcc} = (0,\frac{1}{2},\frac{1}{2})$, demonstrating that an $E_g^{(0)}$ octahedral distortion with C-type wavevector (denoted C-OD) condenses (see Figure 5 (c)/(d) for schematic); lowering the structural symmetry from $Fm\bar{3}m$ to $P4_2/mnm$ (see symmetry lineage in Figure 6) and allowing the C-OO to occur at $U_{\rm Re}$=2.3eV (see Figure 4, panel c). This demonstrates how the C-OD can be an essential ingredient for realizing the orbitally ordered insulating state, by influencing the critical value of $U_{\rm Re}$ for the transition. Incidentally, it should be noted that when the orbital ordering changes, the structural distortion changes as expected. For example, ferro orbital ordering (i.e. F-OO) will lead to a ferro octahedral distortion (i.e. F-OD).

The above analysis proves that it is reasonable to characterize the insulating state as an orbitally ordered state, despite the fact that the C-OD structural distortion could play a critical role in moving the MIT phase boundaries to smaller values of $U_{\rm Re}$. We will demonstrate that this renormalization of the critical $U_{\rm Re}$ via the C-OD allows a common value of $U_{\rm Re}$ to realize the insulating in Sr_2CrReO_6, while retaining a metallic state in Sr_2FeReO_6; and we predict that the orbitally ordered state can persist in the near absence of the C-OD in Ca_2CrReO_6 where electronic correlations are strongest. Given that the C-OD does not occur in the absence $U_{\rm Re}$, we refrain from characterizing this as a Jahn-Teller effect, or pseudo Jahn-Teller effect in the case were the C-OO/C-OD is not a spontaneously broken symmetry,

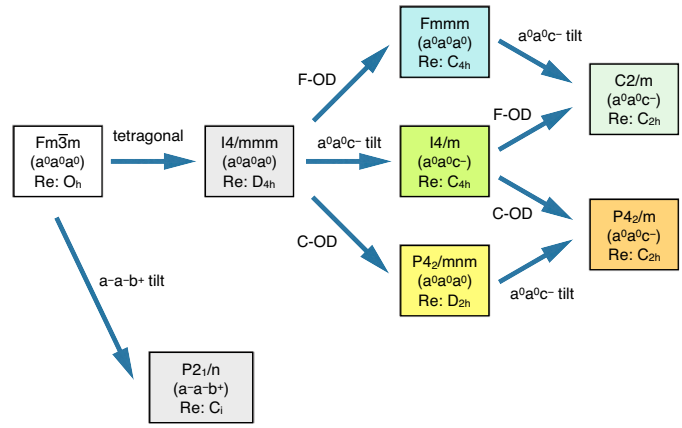

FIG. 6: Hierarchy of the $A_2BB'O_6$ double perovskite space groups connected by various distortions, including octahedral tilts, F-OD, and C-OD. The point group symmetry of the Re site is listed for all structures, along with the octahedral tilt pattern. Ca-based systems follow the $a^-a^-b^+$ arrow, while Sr-based systems proceed along the tetragonal arrow.

which could have been a primary driving force given the orbital degeneracy (or near degeneracy) present in these systems.

Another generic consideration is octahedral tilting, which will influence both the C-OO and the C-OD. The $a^-a^-b^+$ tilt pattern of the Ca-based systems is a relatively large energy scale and therefore the tilts in these system exist independently of orbital ordering and or the C-OD. Alternatively, the $a^0a^0c^-$ tilt pattern of the Sr-based systems is a much weaker energy scale, and therefore it may be somewhat coupled to the orbital ordering and the concomitant C-OD. These statements will be investigated in detail below (see Section III B), where we find that the differences of Sr/Ca are dominant over those of Fe/Cr in terms of setting the effective Re bandwidth; which results in a ordering of Sr_2FeReO_6, Sr_2CrReO_6, Ca_2FeReO_6, Ca_2CrReO_6 (smallest to largest effective Re bandwidth or electronic correlations). For example, the resulting Re-bandwidths are 1.84, 1.70, 1.50, and 1.35 eV, respectively (using $U_{\rm Re}$=0, $U_{\rm Fe}$=4, and $U_{\rm Cr}$=2.5).

Furthermore, the $a^0a^0c^-$ tilt pattern may be isolated from the C-OO/C-OD as they break symmetry in a distinct manner (see symmetry lineage in Figure 6). Therefore, the C-OO/C-OD will be a spontaneously broken symmetry in the Sr based systems (should it occur). Alternatively, the $a^-a^-b^+$ tilt pattern already has a sufficiently low symmetry such that the C-OO/C-OD is not a spontaneously broken symmetry. Therefore, the C-OD cannot strictly be a signature of orbital ordering in the case of the $a^-a^-b^+$ tilt pattern. However, experiment dictates that the magnitude of the C-OD is a useful metric given the discontinuous structural phase transition at 140K between two crystal structures of the same space group ($P2_1/n$, no. 14-2), whereby the magnitude of the C-OD changes discontinuously; and the variant switches

from C-OD$^+$ to C-OD$^-$.

Another generic consideration is the effect of the on-site Coulomb repulsion U for the $3d$ transition metals, which do not nominally have states at low energies given the half filled (sub)shell of (Cr) Fe. However, in reality there is a non-trivial amount of $3d$ states at low energies due to hybridization, more so for Fe than for Cr, and this determines the effective Re-d bandwidth. While $U_{\rm Re}$ can drive orbital ordering even in the absence of $U_{\rm Fe}/U_{\rm Cr}$, as previously illustrated above (see Fig. 4), we will demonstrate the quantitative influence of $U_{\rm Fe}/U_{\rm Cr}$ in renormalizing the critical value of $U_{\rm Re}$ for orbital ordering. First, considering $U_{\rm Re}$=0, one can clearly see an unmixing of $3d$ states from the Re-d states as $U_{\rm Fe}/U_{\rm Cr}$ is applied, further narrowing the effective Re-d bandwidth (compare panels $a \leftrightarrow c$ and $e \leftrightarrow g$ in Fig. 7).

This effect is more dramatic in the case of Fe, which started with a larger degree of hybridization. Focussing on the Fe compound, we see that applying $U_{\rm Re}$=2 does not drive the orbitally ordered insulator even when $U_{\rm Fe}$=4, and thus the system remains metallic despite the diminished Re-d bandwidth. Alternatively, when applying $U_{\rm Re}$=2 to the Cr compound, the addition of $U_{\rm Cr}$=2.5 is sufficient to move the critical value of $U_{\rm Re}$ below 2eV, and an orbitally ordered insulator is obtained. This demonstrates that, while indirect, the on-site U for the $3d$ transition metal can play a critical role. Interestingly, $U_{\rm Cr}$ also turns out to be critical for stabilizing the experimentally observed $a^0a^0c^-$ tilt pattern in Sr_2CrReO_6 (see Section III B 2).

Yet another generic consideration is the spin-orbit coupling. We demonstrate the SOC is a relatively small perturbation in this system by comparing the Re states near the Fermi energy for the cubic reference structure computed using GGA (ie. U=0) with and without SOC (see Fig. 3, panels c and d). As shown, the DOS only exhibits small changes upon introducing SOC. Indeed, we will demonstrate the SOC can shift the phase boundary of the C-OO/C-OD by small amounts, and this can be very relevant in the Ca-based systems (including a strong magnetization direction dependence in Ca_2FeReO_6, see Section III C).

Finally, we discuss how temperature will drive the insulator to metal transition and the structural transition associated with the C-OD. For the most part, we will only address ground state properties in this study, as finite temperatures will be beyond our current scope; though some of our analysis will shed light on what may occur. As outlined above, the insulating ground state in this family of materials is driven by C-type orbital ordering on the Re sites, though two main factors will influence the critical value of $U_{\rm Re}$: the C-OD and octahedral tilting. One can imagine several different scenarios which could play out depending on the energy scales. First, the temperature of the electrons could disorder the C-OO. Given that our DFT+U calculations predict that this C-OO induced insulator is Slater-like (i.e. the gap closes given ferro and other orbital orderings, see Section III B 1 and III B 2), the material will become metallic upon disordering the orbitals. Given that weak nature of the electron-phonon coupling (i.e. the C-OD cannot condense without an on-site $U_{\rm Re}$), this means that the C-OD would disorder along with the orbitals.

TABLE III: Relative energy difference (in meV per formula unit) of the $a^0a^0c^-$ structure minus the $a^0a^0a^0$ structure for Sr_2FeReO_6 within both GGA and GGA+U. The resulting space groups are indicated. We consider full structural relaxations, in addition to only relaxing internal coordinates.

U (eV)	symmetry	inter. rel.	full rel.
$U_{\rm Fe}$=0, $U_{\rm Re}$=0	$I4/m - I4/mmm$	−56	−65
$U_{\rm Fe}$=4, $U_{\rm Re}$=0	$I4/m - I4/mmm$	−44	−51
$U_{\rm Fe}$=0, $U_{\rm Re}$=2	$P4_2/m - P4_2/mnm$	−55	−60
$U_{\rm Fe}$=4, $U_{\rm Re}$=2	$P4_2/m - P4_2/mnm$	−48	−53

A different scenario can be envisioned at an opposite extreme, whereby the energy scale for orbital ordering is very large and we can neglect the electronic temperature and only consider the phonons. In this case, temperature could disorder the C-OD and or the octahedral tilts which would substantially increase the critical value of $U_{\rm Re}$, driving the system into a metallic state. We will entertain this latter scenario (see Section III B, and Figs. 14 in particular), though it does not appear consistent with our preferred values of U when including SOC unless there is a reorientation of the magnetization direction as seen in experiment (see Section III C, and Fig. 20). In reality, it is possible that all ingredients may be needed in order to properly capture the MIT and structural transitions from first-principles, and our paper will lay the groundwork for future study.

B. Crystal and electronic structures

Here we compute the crystal and electronic structure of A_2BReO$_6$ (A=Sr, Ca and B=Cr,Fe), exploring a range of Hubbard Us for all transition metals. We approach the four materials in order of increasing strength of electronic correlations: Sr_2FeReO_6, Sr_2CrReO_6, Ca_2FeReO_6, Ca_2CrReO_6. We will address orbital ordering, axial octahedral distortions, octahedral tilt pattern, the presence of a band gap, and relative structural energetics.

1. Sr_2FeReO_6

Experimentally, Sr_2FeReO_6 is found to be a metal with an $a^0a^0c^-$ octahedral tilt pattern and $I4/m$ symmetry (see Section I B). Given that Sr will have a smaller propensity to drive octahedral tilts relative to Ca, and that in Figure 3 we showed that Re has a larger effective

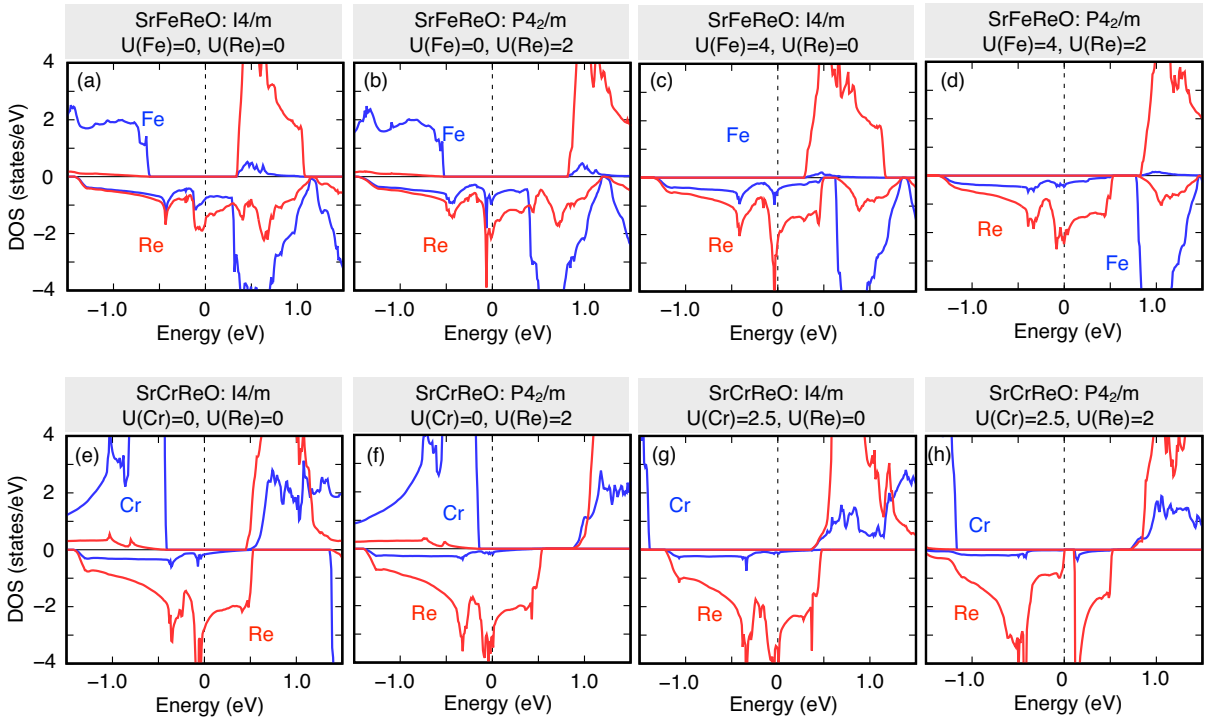

FIG. 7: Projected density of states of Sr_2CrReO_6 and Sr_2FeReO_6, projected on Fe (blue), Cr (blue), and Re (red) d orbitals. Values of U and space group (obtained from relaxing internal coordinates) are indicated in each panel.

bandwidth in Fe based systems as opposed to Cr based systems, it is easy to understand why Sr_2FeReO_6 is the only metal among the four compounds considered.

Here we explore the interplay of octahedral tilts, octahedral distortions, and the Hubbard U in detail (see Fig. 8); including at least six different crystal structures (i.e. all structures in Fig. 6 except $Fm\bar{3}m$ and $P2_1/n$). We will use the acronym OD (i.e. octahedral distortion) to generically refer to any spatial ordering of $E_g^{(0)}$ octahedral distortions ($E_g^{(0)}$ is shown schematically in Fig. 5, panels c, d and mathematically defined in Ref.[100]), such as C-OD for C-type ordering, F-OD for ferro ordering, etc; and the same nomenclature will be used for the orbital ordering (i.e. OO generically refers to C-OO, F-OO, etc.). In the higher symmetry structures which lack an OD (i.e. $I4/m$ and $I4/mmm$), the Hubbard U may cause the electrons to spontaneously break space group symmetry despite the fact that we will prevent the nuclei from breaking symmetry; allowing us to disentangle different effects. This is achieved by using a reference crystal structure obtained from relaxing with $U_{\rm Re}$=0 and then retaining this structure for $U_{\rm Re}$ >0 (this process is repeated for different values of $U_{\rm Fe}/U_{\rm Cr}$). Anytime a reference structure is employed, it will be indicated using an asterisk. Given that the OO/OD is a spontaneously broken symmetry for $I4/m$, we could have created a reference structure simply by enforcing space group symmetry, but this is not possible in the Ca-based systems where the OO/OD is not a spontaneously broken symmetry; and we prefer to have a uniform approach throughout.

We note that in all cases we retain the small degree of tetragonality in the lattice parameters, so there is technically always a very small tetragonal distortion ($\sqrt{2}a$=7.865 and c=7.901[1]). Fully relaxing the lattice parameters had a very small effect on the results in the test cases we evaluated (see Table III). In all panels, solid points indicate an insulator, while hollow points indicate a metal.

It should be noted that the structures with an OO (e.g. C-OO, F-OO, etc.) are merged into the same line for brevity, despite the fact that they have different space groups (see Fig. 6). The C-OO can easily be distinguished as it is always insulating in this compound (it is only favorable at larger values of $U_{\rm Re}$), and the F-OO is always metallic (it is only favorable at smaller values of $U_{\rm Re}$). The same statements clearly follow for C-OD and F-OD, given that the orbital ordering is what causes the structural distortion. Interestingly, we will show that there is a different state which can occur at intermediate values of $U_{\rm Re}$ in the region between the F-OO/F-OD and the C-OO/C-OD, and this is a ferrimagnetic orbital ordering (FI-OO) and corresponding octahedral distortion (FI-OD); though the smaller magnitude OO/OD within the FI-OO/FI-OD is always nearly zero. These three regimes, F-OO/F-OD, FI-OO/FI-OD, and C-OO/C-OD, are easy to identify due to kinks in the curves, as we shall

point out. The FI-OD will prove not to be important given that it tends to lose a competition with octahedral tilting. For each structure, we present the relative energy ΔE (i.e. the energy of a reference structure with respect to the ground state, panels a and b), the band gap (panel b,c), the amplitude of the OD (denoted $d_{|x-y|}$, see panel d,e), and the magnitude of the OO defined as the orbital polarization (panels f and g):

$$P_{xz,yz} = \frac{1}{N_\tau} \sum_\tau \frac{|n^\tau_{d_{yz}} - n^\tau_{d_{xz}}|}{n^\tau_{d_{yz}} + n^\tau_{d_{xz}}} \quad (1)$$

where n^τ_d is the occupancy of a given minority spin d orbital, τ labels a Re site in the unit cell, and N_τ is the number of Re atoms in the unit cell.

We first focus on the left column of panels in Fig. 8 (i.e. a, c, e, and g), where $U_{\rm Fe}$=4, though nearly qualitative behavior is independent of $U_{\rm Fe}$; the few small differences will be noted as they arise. Focussing on the blue curves corresponding to the $*a^0a^0a^0$ structure (where the nuclei are constrained to space group $I4/mmm$), we see that $d_{|x-y|}$ is zero, as it must be when the nuclei are confined to this space group. Despite this fact, $P_{xz,yz}$ reveals a small symmetry breaking of the electronic density for $U_{\rm Re}$ $\leq$2.2 (see panel g) where F-OO is found; and this sharply transitions to a new plateau for 2.3$\leq$ $U_{\rm Re}$ $\leq$2.7 where FI-OO is found; and finally there is a sharp transition to the C-OO insulating state for $U_{\rm Re}$ $\geq$2.8. Therefore, the MIT occurs at approximately $U_{\rm Re}$=2.8 in this scenario. Inspecting the relative energy, ΔE is roughly constant up until approximately $U_{\rm Re}$=2, whereafter ΔE increases linearly due to the fact that the ground state structure has formed the C-OO/C-OD.

Allowing the C-OD to condense, but still in the absence of tilts, will shift the orbital ordering to lower values of $U_{\rm Re}$; and this is illustrated in the red curves labeled $a^0a^0a^0$+OD (space group $Fmmm$ and $P4_2/mnm$ for the F-OD and C-OD, respectively). A jump in the value of the OD amplitude $d_{|x-y|}$ can be seen occurring concomitantly with the orbital polarization. Clearly, the C-OD cooperates with the C-OO, allowing the latter to form at smaller values of $U_{\rm Re}$ and saturate at larger values. Here ΔE has two clear kinks in the slope, given that the curve begins as roughly constant, then changes to linear when the ground state forms the C-OO/C-OD, and then becomes constant once again when the C-OO/C-OD forms in this $a^0a^0a^0$+OD structure.

We can now explore the results where we allow $a^0a^0c^-$ tilts, but not the OD (ie. nuclei are frozen in $I4/m$ space group, see green curves labeled $*a^0a^0c^-$). The tilts also reduce the threshold $U_{\rm Re}$ needed to drive the C-OO insulating state as compared to the $*a^0a^0a^0$ reference structure. Serendipitously, this reduction is roughly the same as the $a^0a^0a^0$+OD reference structure; though we see that when comparing the energetics of these two cases, $*a^0a^0c^-$ is favorable up to the largest $U_{\rm Re}$ considered (see panel a). It should be noted that the ferri FI-OO state is not realized in this case (ie. F-OO transitions directly to C-OO).

TABLE IV: Magnetic moment M (μ_B) and N_d of Cr/Fe and Re atoms in Re-DPs within GGA and GGA+U, where $U_{\rm Cr}$=2.5, $U_{\rm Fe}$=4, and $U_{\rm Re}$=2.

	M(Cr/Fe)		M(Re)	
	GGA	GGA+U	GGA	GGA+U
Sr_2FeReO_6	3.647	4.086	0.815	1.340
Sr_2CrReO_6	2.239	2.647	1.068	1.532
Ca_2FeReO_6	3.593	4.094	0.804	1.411
Ca_2CrReO_6	2.329	2.689	1.135	1.581
	N_d(Cr/Fe)		N_d(Re)	
	GGA	GGA+U	GGA	GGA+U
Sr_2FeReO_6	5.896	5.743	4.178	4.140
Sr_2CrReO_6	4.131	4.075	4.251	4.210
Ca_2FeReO_6	5.884	5.717	4.171	4.152
Ca_2CrReO_6	4.107	4.031	4.229	4.194

Finally, we can allow both $a^0a^0c^-$ tilts and the OD (ie. space group $P4_2/m$, see black curves labeled $a^0a^0c^-$+OD), which cooperate to strongly reduce the threshold for the C-OO insulating state to $U_{\rm Re}$=2.1. Interestingly, this appears to occur because the tilts have a preference for converting the FI-OD to the C-OD (see panels e and g), which appears reasonable given that the tilt pattern of the Re alternates in the z-direction with the same phase as the C-OD. All of the same generic trends can be observed in the right column where $U_{\rm Fe}$=0, though all transitions are shifted to higher values of $U_{\rm Re}$ as is expected for a larger effective Re bandwidth.

Given that Sr_2FeReO_6 is metallic in experiment, and that we expect $U_{\rm Fe}$=4 to be a reasonable value, we would infer that $U_{\rm Re}$ $\leq$2.0 in order to be consistent with experiment (see Section III D for a more detailed discussion). In the region $U_{\rm Re}$ $\leq$2.0, the energy differences are nearly constant, and it is worth noting that the predicted energy gain for octahedral tilting is reasonable given the experimentally observed transition from $I4/m \rightarrow Fm\bar{3}m$ at $T = 490K$.

It is also useful to determine the effect of U on the magnetic moment of the transition metal sites in addition to the number of electrons (N_d) in the correlated manifold (see Table IV). The Fe and Re moments are 3.65 (4.09) and 0.82 (1.34) μ_B, respectively, within GGA (GGA+U). The number of d electrons decreases by roughly 0.15 electrons for Fe as U is turned on, reflecting the unmixing the Fe; while the changes in Re are more modest.

2. Sr_2CrReO_6

As we discussed in the literature review (see Section I B), several experiments suggested that Sr_2CrReO_6 is metallic with space group $I4/m$ (demanding that

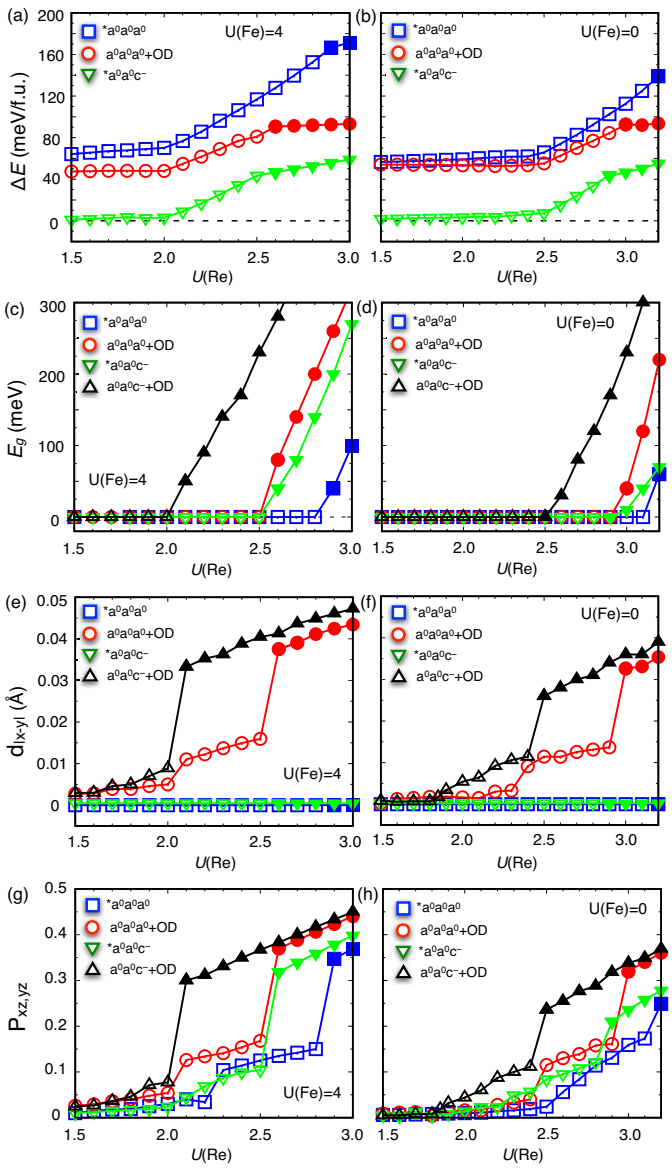

FIG. 8: (a),(b) Relative energy of Sr_2FeReO_6 in several structures with respect to the ground state (i.e. $a^0a^0c^-$+OD). (c),(d) Electronic band gaps of different phases of Sr_2FeReO_6. (e),(f) Octahedral distortion (OD) amplitude $d_{|x-y|}$ of the ReO_6 octahedron. (g),(h) Orbital polarization $P(d_{xz}, d_{yz})$ (see eq. 1) for Re. Panels (a), (c), (e), and (g) correspond to $U_{\rm Fe}$=4, while panels (b), (d), (f), and (h) correspond to $U_{\rm Fe}$=0. Filled and empty points stand for the insulating and metallic phases, respectively.

$d_{|x-y|}$=0)[1,2,29,30]. However, recently Hauser *et al.* proposed that a fully-ordered Sr_2CrReO_6 film on the STO substrate is in fact a semiconductor with $E_{\rm gap}$=0.21 eV[3], and further suggested that the previously reported metallicity of Sr_2CrReO_6 may be due to oxygen vacancies[27]. Our calculations lend support to the observations of Hauser *et al.*, showing that the C-OO/C-OD can induce an insulating state for reasonable values of $U_{\rm Re}$.

Here we perform the same analysis for Sr_2CrReO_6 as in the previous section for Sr_2FeReO_6, demonstrating the same generic behavior; but different quantitative thresholds (see Fig. 9). The main notable difference observed in Sr_2CrReO_6 as compared to Sr_2FeReO_6 is the energy scale for octahedral tilting, where $U_{\rm Cr}$ plays a role in stabilizing the tilt pattern. For example, when $U_{\rm Cr}$=0 octahedral tilting is either unstable or stabilized by less than 1meV, depending on whether or not one relaxes lattice parameters in addition to internal coordinates (see Table V). However, applying a non-zero $U_{\rm Cr}$ results in a small stabilization energy for $a^0a^0c^-$ tilting, and this effect only depends weakly on $U_{\rm Re}$ prior to the onset of the C-OO (i.e. $U_{\rm Re} < 2$; see Fig. 9, panels a and b). Clearly, a non-zero $U_{\rm Cr}$ is essential to obtaining an energy scale for octahedral tilting which is consistent with a tilt transition of T = 260K (see Table I). Otherwise, all of the same trends from Sr_2FeReO_6 can be seen in Sr_2CrReO_6. If we then take a value of $U_{\rm Cr}$=2.5, an insulating state can only be achieved if $U_{\rm Re} \gtrsim 2$ for the ground state structure $P4_2/m$ (i.e. $a^0a^0c^-$+C-OD).

Given our preferred values of U (i.e. $U_{\rm Cr}$=2.5 and $U_{\rm Re}$=2), Sr_2CrReO_6 is insulating as in experiment. However, given these values of U, the C-OD is a necessary condition for realizing the insulating state (i.e. compare the black and green curves in Fig. 9, panel c), and the C-OD is only energetically favorable by 5.5 meV (i.e. green curve in panel a). Therefore, if thermal fluctuations of the phonons were to disorder the C-OD, the system would be driven through the MIT. The system could remain insulating in the absence of the C-OD if $U_{\rm Re} \gtrsim 2.4$, but then Sr_2FeReO_6 would be insulating with a C-OD stabilized by 34.4 meV for $U_{\rm Re}$ = 2.4; inconsistent with experiment. Therefore, the C-OD should condense at sufficiently low temperatures in experiment and the space group should be measured to be $P4_2/m$ instead of $I4/m$ given sufficiently clean samples. Later we demonstrate that SOC introduces quantitative changes, but the same general conclusion holds. Future experiments can test this prediction.

Given that the experimental insulating state was realized via growth on STO, it is worthwhile to determine the influence of imposing the STO lattice parameter (a=3.905); which is ∼0.04% of compressive strain compared to the optimized lattice parameter within GGA+U (with $U_{\rm Cr}$=2.5 and $U_{\rm Re}$=2). We find that this strain has only a small effect on energy differences, resulting in a difference of −17.8 meV for $P4_2/m - P4_2/mnm$, as compared to −18.5 meV for the bulk case in Table V; and therefore we do not believe the substrate has any substantial effect.

The magnetic moments and number of electrons as a function of U are summarized in Table IV. The Cr and Re moments are 2.24 (2.65) and 1.07 (1.53) μ_B, respectively, within GGA (GGA+U). However, note that the total moment is constant ($1\mu_B$/f.u.) within both GGA and GGA+U. The number of d electrons decreases by

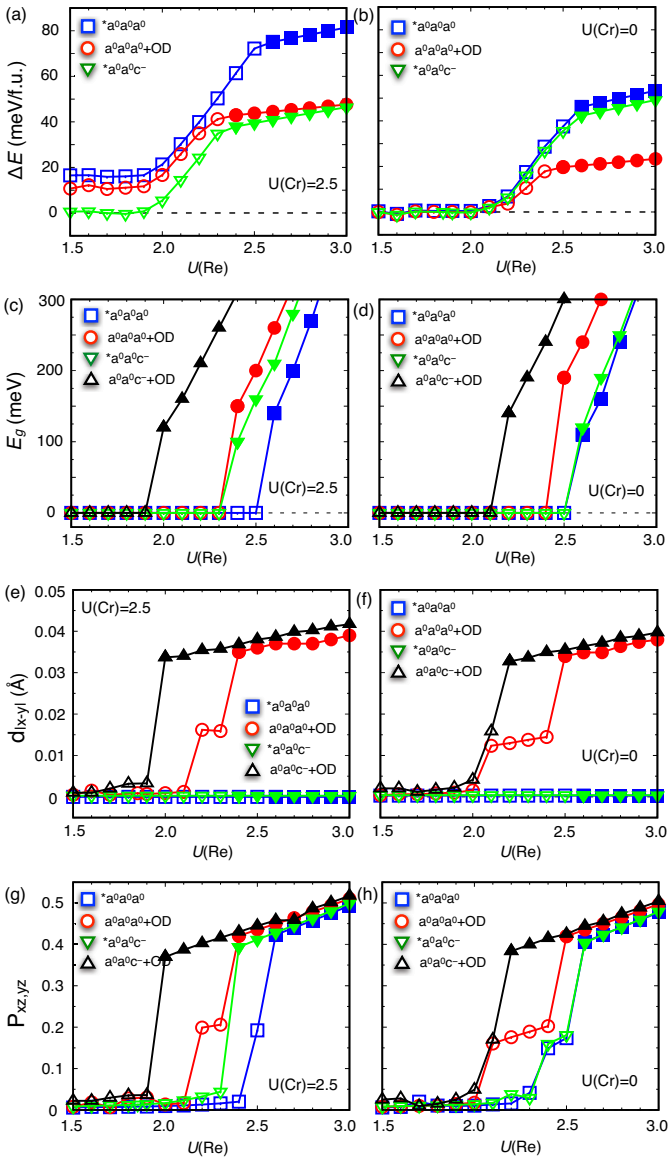

FIG. 9: (a),(b) Relative energy of Sr_2CrReO_6 in several structures with respect to the ground state (ie. $a^0a^0c^-$+OD). (c),(d) Electronic band gaps of different phases of Sr_2CrReO_6. (e),(f) Octahedral distortion (OD) amplitude $d_{|x-y|}$ of the ReO_6 octahedron. (g),(h) Orbital polarization $P(d_{xz}, d_{yz})$ (see eq. 1) for Re. Panels (a), (c), (e), and (g) correspond to $U_{\rm Cr}$=2.5, while panels (b), (d), (f), and (h) correspond to $U_{\rm Cr}$=0. Filled and empty points stand for the insulating and metallic phases, respectively.

∼0.06 for Cr as U is turned on, which is almost half of the change of N_d of Fe in Sr_2FeReO_6. Smaller change of N_d(Cr) also reflects the weaker Cr-Re hybridization.

TABLE V: Relative energy difference (in meV per formula unit) of the $a^0a^0c^-$ structure minus $a^0a^0a^0$ for Sr_2CrReO_6 within both the GGA and GGA+U calculations, and their crystal symmetries. We consider full structural relaxations, in addition to only relaxing internal coordinates.

U(eV)	symmetry	inter. rel.	full rel.
$U_{\rm Cr}$=0, $U_{\rm Re}$=0	$I4/m - I4/mmm$	0.07	−0.06
$U_{\rm Cr}$=2.5, $U_{\rm Re}$=0	$I4/m - I4/mmm$	−4.90	−7.96
$U_{\rm Cr}$=3.5, $U_{\rm Re}$=0	$I4/m - I4/mmm$	−11.90	−13.89
$U_{\rm Cr}$=0, $U_{\rm Re}$=2	$P4_2/m - P4_2/mnm$	−0.33	−0.48
$U_{\rm Cr}$=2.5, $U_{\rm Re}$=2	$P4_2/m - P4_2/mnm$	−18.47	−20.45
$U_{\rm Cr}$=3.5, $U_{\rm Re}$=2	$P4_2/m - P4_2/mnm$	−29.67	−28.98

TABLE VI: Nonzero octahedral modes of ReO_6 in Ca_2FeReO_6, for one of the two symmetry equivalent Re atoms in the unit cell. The mathematical definition of each mode can be found in Figure 4 of Ref.[100]. The local coordinate system is chosen by having zero rotation modes (i.e., amplitude of T_{1g} modes are zero). The amplitudes for the other Re-O octahedron in the corresponding local coordinate system can be obtained by inverting the sign of $E_g^{(0)}$, and swapping the values of $T_{2g}^{(1)}$ and $T_{2g}^{(2)}$. It should be noted that the low and high temperature experimental structures are different C-OD variants.

	exp[16]		GGA		
modes	7K	300K	GGA	+U	+U+SOC
A_{1g}	4.7834	4.7780	4.7655	4.8077	4.8146
$E_g^{(0)}$	−0.0137	−0.0046	−0.0017	−0.0335	−0.0260
$E_g^{(1)}$	−0.0126	−0.0196	−0.0066	−0.0171	−0.0012
$T_{2g}^{(0)}$	0.0005	0.0179	0.0109	0.0022	0.0078
$T_{2g}^{(1)}$	−0.0423	0.0192	−0.0293	−0.0678	−0.0582
$T_{2g}^{(2)}$	0.0225	−0.0255	0.0205	0.0256	0.0271

3. Ca_2FeReO_6

We now move on to the case of Ca_2FeReO_6, which has the lower symmetry space group $P2_1/n$ ($a^-a^-b^+$ tilt, see Fig. 1) and is measured to be an insulator with a 50meV energy gap at low temperature (see Section I B for a detailed review). Given the smaller size of Ca relative to Sr, the tilts in both Ca-based materials are large in magnitude (see Table VI for octahedral mode amplitudes) and retained up to the highest temperatures that have been studied in experiment (i.e. 300K and 550K for Ca_2CrReO_6 and Ca_2FeReO_6, respectively). For example, two in-plane and one out-of-plane ∠Fe-O-Re are 151.2, 151.8, and 152.4° at 7K, and both DFT and DFT+U accurately capture the large magnitude of the octahedral tilts: ∠Fe-O-Re are 149.9, 151.1, 150.5 using DFT; 149.7, 150.0, and 150.8° using DFT+U ($U_{\rm Fe}$=4 and $U_{\rm Re}$=2).

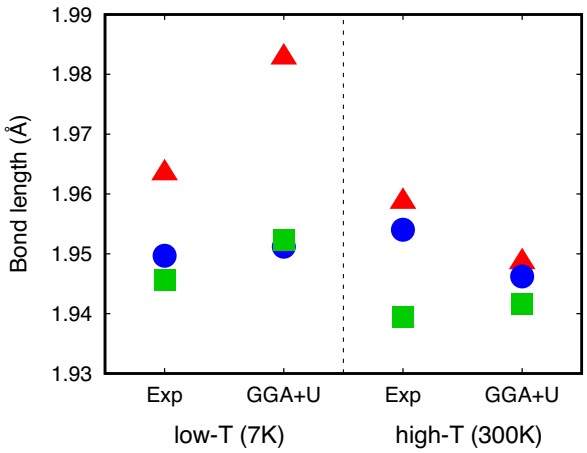

FIG. 10: Re1–O bond lengths of Ca_2FeReO_6 for the experimental structures at high- and low-temperature[16], and from the relaxed structures within GGA and GGA+U. Blue circle, red triangle, and green box stand for Re1–O1, Re1–O2, and Re1–O3, respectively, where Re1–O3 is the out-of-plane Re–O bond. The Re2–O bond lengths are given by Re2–O1=Re1–O2, Re2–O2=Re1–O1, and Re2–O3=Re1–O3. Given our unit cell conventions (see Fig. 11), the experimental paper plots Re1–O in the low temperature phase and Re2–O in the high temperature phase.

Furthermore, these large tilts substantially reduce the effective Re bandwidth, resulting in a smaller critical value of $U_{\rm Re}$ needed to drive the C-OO induced insulating state, as we will now illustrate.

In Sec. I B, we briefly discussed the structures of Ca_2FeReO_6 obtained at low and high temperatures[16], as summarized in Fig. 10. According to experiment, there is an appreciable C-OD amplitude below the phase transition (e.g. C-OD$^+$, $d_{|x-y|} = 0.014\AA$ at T=7K), and it is highly suppressed and swapped to the alternate variant above the transition temperature of $T = 140K$ (e.g. C-OD$^-$, $d_{|x-y|} = 0.005\AA$ at T=300K). It should be emphasized that the C-OD is not a spontaneously broken symmetry in this structure, in contrast to the Sr case (see symmetry lineage in Fig. 6).

We now elaborate on the fact that there are two types of C-OD within the monoclinic $P2_1/n$ structure (see schematic in Fig. 11). We will use a notation of C-OD$^+$ to denote the ordering where a given Re-O octahedron has the same sign for the $E_g^{(0)}$ mode (defined in the unrotated coordinate system) and the rotation mode (i.e. both modes positive or both modes negative); whereas C-OD$^-$ indicates opposite signs. Structures below and above the MIT exhibit C-OD$^+$ and C-OD$^-$, respectively. Note that the C-OD$^+$ and C-OD$^-$ are distinguishable only in the monoclinic (i.e., $a \neq b$) double perovskites, whereas they are symmetry equivalent in the tetragonal double perovskites (e.g. in the Sr-based systems).

GGA results in C-OD$^+$, and C-OD$^-$ is not even metastable (i.e. it relaxes back to C-OD$^+$); though the C-OD$^+$ amplitude is negligibly small (i.e., $d_{|x-y|} <$

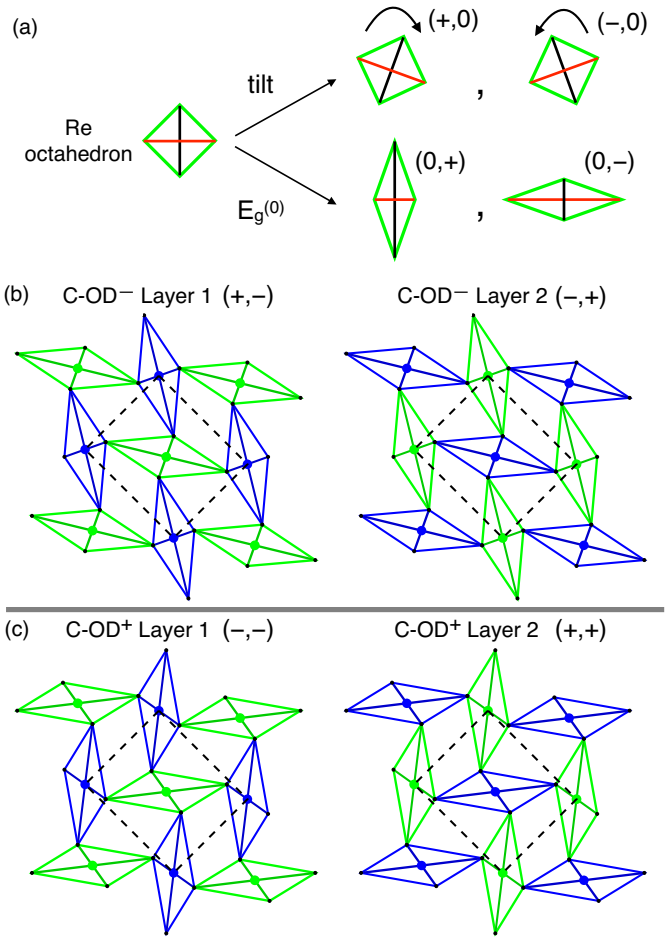

FIG. 11: (a) Signs of the tilt mode (clockwise being positive) and $E_g^{(0)}$ mode (y elongation being positive) of Re-O octahedron. Black and red lines correspond to Re-O bonds. Quantities in parenthesis, give the sign of the tilt and $E_g^{(0)}$ amplitude, respectively. (b), (c) Two dimensional schematic of the two possible orientations of C-OD: C-OD$^-$ and C-OD$^+$. Black dots represent oxygen, green dots represent Re, and blue dots represent B atom (Fe or Cr). The dashed rectangle is the unit cell, where $a < b$. The coordinate system is the same as depicted in Fig. 5. Each schematic is defined by three numbers: the tetragonality of the unit cell, the octahedral tilt amplitude, and the amplitude of the $E_g^{(0)}$ mode. Panels (a) and (b) (i.e. C-OD$^-$ and C-OD$^+$, respectively) only differ in the sign of the octahedral tilt amplitude. The amplitudes of the distortions are exaggerated to showcase the difference between C-OD$^+$ and C-OD$^-$.

$0.001\AA$). The energies of C-OD$^+$ and C-OD$^-$ become distinct as $U_{\rm Re}$ increases, while the relative stability also depends on $U_{\rm Fe}$. As depicted in Fig. 12(a), C-OD$^+$ switches to C-OD$^-$ at $U_{\rm Re}$=1.4 when $U_{\rm Fe}$=4, and the energy difference increases as a function of $U_{\rm Re}$. When $U_{\rm Fe}$=0, as shown in Fig. 12(b), C-OD$^+$ is always favorable, and its stability increases in the range $U_{\rm Re}$=1.8−2.5eV. Since the energy difference between two different orderings is very small, we simply follow C-OD$^+$ (i.e. low tempera-

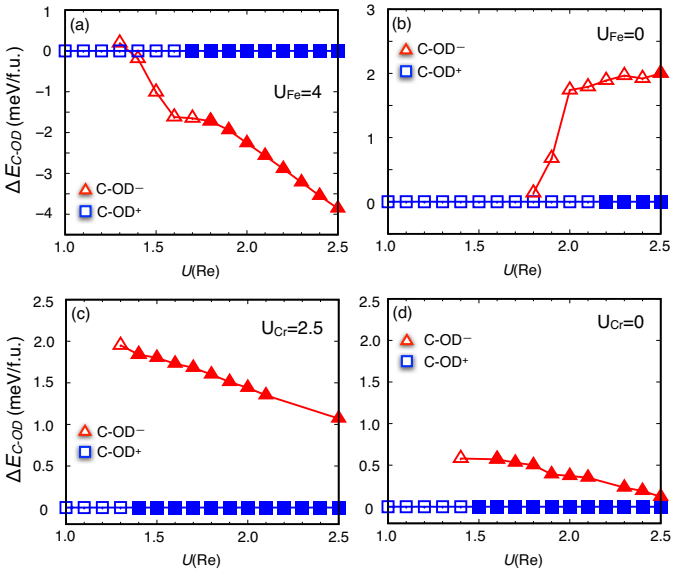

FIG. 12: Energies for C-OD$^+$ (blue square) and C-OD$^-$ (red triangle) relative to C-OD$^+$ as a function of U_{Re}. (a),(b) Ca_2FeReO_6 with U_{Fe}=4 and U_{Fe}=0, respectively. (c),(d) Ca_2CrReO_6 with U_{Cr}=2.5 and U_{Cr}=0, respectively. Empty and filled points stand for metallic and insulating phases, respectively.

ture orientation) whenever applying DFT+U. In terms of the C-OD amplitudes, GGA+U and GGA agree more closely for the low-T and high-T structures, respectively (see Figure 10), though GGA+U overestimates and GGA underestimates $d_{|x-y|}$.

We now perform the same analysis as for the Sr-based systems, except that the untilted structure does not need to be considered given its large energy scale. In the Sr-based systems, we considered high symmetry reference structures, where we allowed the electrons to spontaneously break symmetry but prevented the structure from doing so by fixing it at the relaxed U_{Re}=0 structure (though non-zero $U_{\mathrm{Cr}}/U_{\mathrm{Fe}}$ was included in creating a relaxed reference structure). The same recipe can be followed in the Ca-based cases, despite the fact that the U_{Re}=0 structure has an identical space group symmetry, and this reference structure will be referred to as $*a^-a^-b^+$; where the asterisk indicates that this a reference structure where we have effectively removed the C-OD which is induced by orbital ordering. Comparison to the reference structure will give insight into the importance of the C-OD in realizing the C-OO. Additionally, we will also study the unrelaxed experimentally measured structures from T=120K and T=160K, which straddle the T=140K phase transition. Due to the strong octahedral tilting, only the C-OO/C-OD is found in the Ca-based results, as opposed the Sr-based systems where ferro and ferri OO/OD's are observed.

We begin by focussing on the reference structure $*a^-a^-b^+$, depicted by a green curve, where the C-OD amplitude is negligibly small irrespective of U_{Fe} (see Fig.

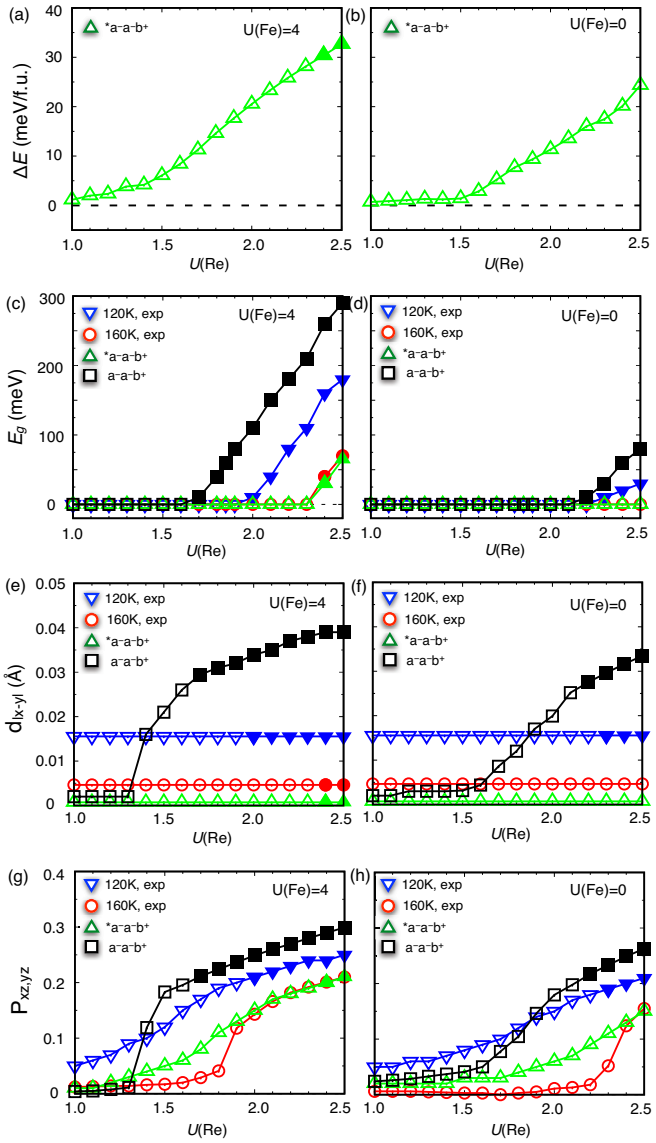

FIG. 13: (a),(b) Relative energy of Ca_2FeReO_6 in the reference structure $*a^-a^-b^+$ (where the C-OD amplitude is suppressed, see text) with respect to the ground state (ie. $a^-a^-b^+$). (c),(d) Electronic band gaps of different phases. (e),(f) Octahedral distortion (OD) amplitude $d_{|x-y|}$ of the ReO_6 octahedron. (g),(h) Orbital polarization $P(d_{xz}, d_{yz})$ (see eq. 1) for Re. Panels (a), (c), (e), and (g) correspond to U_{Fe}=4, while panels (b), (d), (f), and (h) correspond to U_{Fe}=0. Filled and empty points stand for the insulating and metallic phases, respectively. The frozen experimental structures at 120K and 160K[16], which bound the phase transition, are included for comparison.

13, panels e and f). Increasing U_{Re} causes the orbital polarization to increase, and an insulating state (solid point) is eventually realized at U_{Re}=2.4 for the case of U_{Fe}=4 (see Fig. 13, panels c, e, and g). For U_{Fe}=4, the relative energy ΔE increases rather slowly for $U_{\mathrm{Re}} \lessapprox 1.4$, and the slope increases thereafter due to the fact that the

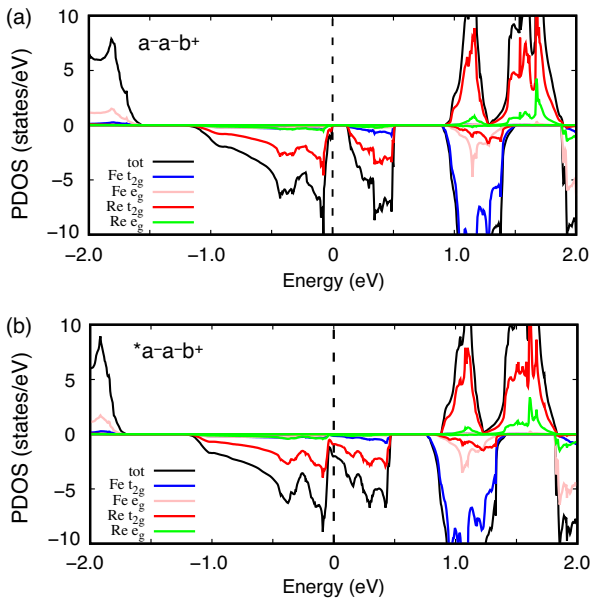

FIG. 14: DFT+U projected density of states of Ca_2FeReO_6 (a) in the ground state structure ($a^-a^-b^+$) (b) in the reference structure $*a^-a^-b^+$. The Fermi energy is set to be zero; $U_{\rm Re}$=2.0 and $U_{\rm Fe}$=4.

ground state experiences the C-OO/C-OD at $U_{\rm Re} \approx 1.4$. As in Sr-based systems, turning off the U on the $3d$ transition metal shifts the metal-insulator phase boundary to larger values of $U_{\rm Re}$, and an insulating state is not achieved for $U_{\rm Re}$ $\leq$2.5 if $U_{\rm Fe}$=0 (panels d, f, and h). Hereafter we focus our discussion on $U_{\rm Fe}$=4, as all the same qualitative trends hold upon decreasing $U_{\rm Fe}$. The experimental T=160K structure (depicted by a red curve) shows relatively small differences as compared to the $*a^-a^-b^+$ reference structure, with the band gap being quantitatively similar.

We now move on to the fully relaxed structure, where C-OD amplitude is allowed to relax as $U_{\rm Re}$ is increased (depicted as black curve). In this discussion, we focus on $U_{\rm Fe}$=4. For $U_{\rm Re}$ $\leq$1.3, both the orbital polarization (i.e. $P_{xz,yz}$) and the C-OD amplitude (i.e. $d_{|x-y|}$) are very small with a weak $U_{\rm Re}$ dependence; comparable in magnitude to the reference structure. Once $U_{\rm Re}$ >1.3, there is a sharp increase in the C-OO/C-OD amplitude, and the system becomes an insulator for $U_{\rm Re}$ $\geq$1.7. Therefore, the cooperation of the C-OO and C-OD greatly reduces the critical $U_{\rm Re}$ needed to drive the insulating state, from a value of $U_{\rm Re}$=2.4 in the reference $*a^-a^-b^+$ structure down to a value of 1.7; which is the same trend as the case of the Sr-based systems. It is interesting to compare the relaxed C-OD amplitude to that of the T=120K experimental structure, depicted as a blue curve. In the relaxed structure, the smallest value of $U_{\rm Re}$ which has an insulating state is 1.7, and already the C-OD amplitude is nearly twice that of the experimental T=120K structure. However, later we demonstrate that including SOC dampens the C-OD amplitude (though not enough to agree with experiment, see Section III C, Fig. 19). The T=120K and T=160K experimental structures produce a critical $U_{\rm Re}$ of 2.0 and 2.4 for the C-OO/C-OD, respectively, which is still appreciably different.

Given the substantial renormalization of the critical $U_{\rm Re}$ between the $*a^-a^-b^+$ reference structure and the fully relaxed structure, and analogously between the two experimental structures, it is interesting to consider the possibility of the anharmonic phonon free energy being the primary driving force of the MIT as a function of temperature. In this scenario, the structural transition is driven by the phonon free energy, and the resulting change in the structure is sufficient to renormalize the critical value of $U_{\rm Re}$ and drive the system through the MIT.

Using our prescribed values of $U_{\rm Re}$=2.0 and $U_{\rm Fe}$=4 (given that we are not yet using spin-orbit coupling), we plot the site/orbital projected electronic density-of-states for the $*a^-a^-b^+$ reference structure and the relaxed $a^-a^-b^+$ structure (see Fig. 14). As shown, the result is a metal for the $*a^-a^-b^+$ structure and an insulator for the $a^-a^-b^+$ structure, with the latter having a gap of 110meV; slightly larger than relatively small experimental gap of 50meV. While a greater value of $U_{\rm Re}$ would yield an insulator in the $*a^-a^-b^+$ structure, this sort of tuning is discouraged by the fact that Sr_2FeReO_6 would wrongly be driven into a C-OO/C-OD insulating state in contradiction with experiment (assuming a common value of $U_{\rm Re}$ is utilized). Future work will determine if this phonon driven scenario is dominant, as opposed to the other extreme where temperature disorders the electrons (see Section III A for further discussion of these scenarios).

4. Ca_2CrReO_6

Similar to Ca_2FeReO_6, Ca_2CrReO_6 results in a monoclinic structure $P2_1/n$ ($a^-a^-b^+$ tilt, see Fig. 1) with an insulating ground state. Both DFT and DFT+U reasonably capture the large magnitude of the octahedral tilts: the two in-plane and one out-of-plane ∠Cr-O-Re are 153.8, 154.1, 154.9 using DFT; 151.7, 151.0 and 152.7° using DFT+U ($U_{\rm Cr}$=2.5 and $U_{\rm Re}$=2); and 153.1, 154.3, and 155.0° as measured at T=300K in experiment[1]. In terms of the C-OD amplitude, the experimental value of $d_{|x-y|}$ at 300K reported by Kato *et al.* is 0.003 Å, which is smaller than $d_{|x-y|}$ = 0.005$\AA$ of Ca_2FeReO_6 at the same temperature[1]; and this suggests that the C-OD has been disordered at 300K, yet the transport still suggests an insulating state. Unfortunately, the low temperature values of $d_{|x-y|}$ have not yet been measured, but we will demonstrate that a large C-OD amplitude is expected just as in the case of Ca_2FeReO_6.

Just as in the case of Ca_2FeReO_6, the C-OD may form in either the C-OD$^+$ or C-OD$^-$ variant. Unlike Ca_2FeReO_6, C-OD$^+$ ordering is more stable over a broad

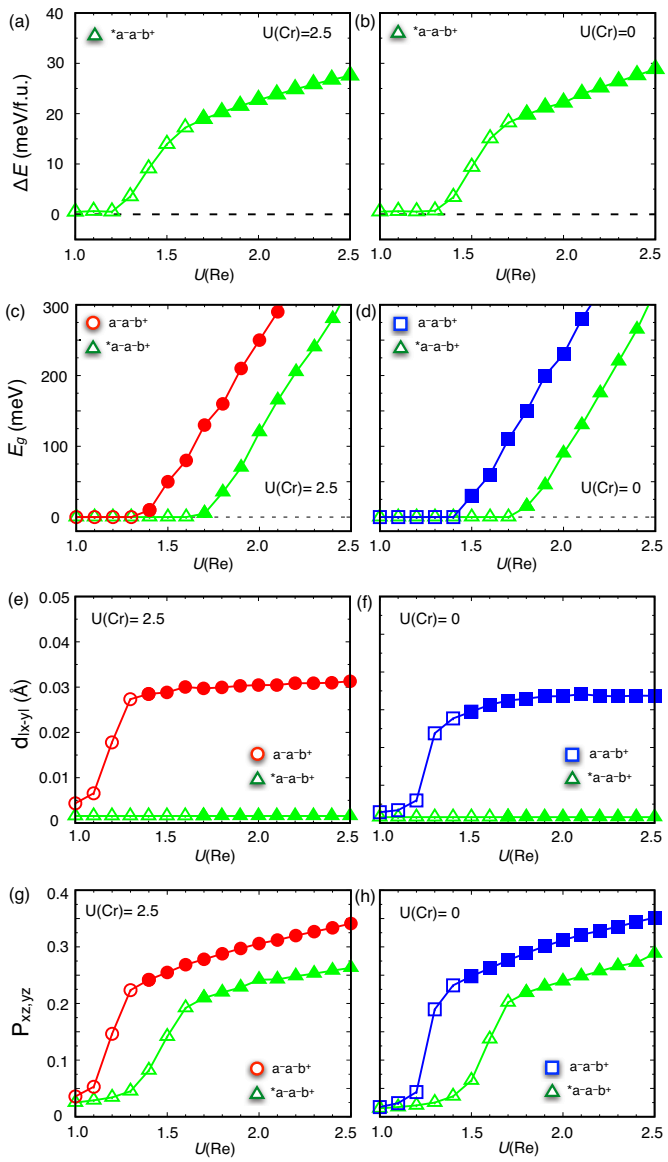

FIG. 15: (a),(b) Relative energy of Ca_2CrReO_6 in the reference structure $*a^-a^-b^+$ (where the C-OD amplitude is suppressed, see text) with respect to the ground state (i.e. $a^-a^-b^+$). (c),(d) Electronic band gaps of different phases. (e),(f) Octahedral distortion (OD) amplitude $d_{|x-y|}$ of the ReO_6 octahedron. (g),(h) Orbital polarization $P(d_{xz}, d_{yz})$ (see eq. 1) for Re. Panels (a), (c), (e), and (g) correspond to $U_{\rm Cr}$=2.5, while panels (b), (d), (f), and (h) correspond to $U_{\rm Cr}$=0. Filled and empty points stand for the insulating and metallic phases, respectively.

range of $U_{\rm Re}$, as depicted in Figs. 12. The energy difference between the C-OD variants are relatively small as compared to the case of Ca_2FeReO_6, which might be due to the smaller difference between the respective a and b lattice parameters. More specifically, $b-a$ is 0.070$\AA$ in Ca_2FeReO_6, while $b-a$ is 0.026$\AA$ in Ca_2CrReO_6. In both cases, the energy difference between C-OD$^+$/C-OD$^-$ is well within the error of DFT+U. As in the case of Ca_2FeReO_6, here we only present the results of C-OD$^+$ ordering.

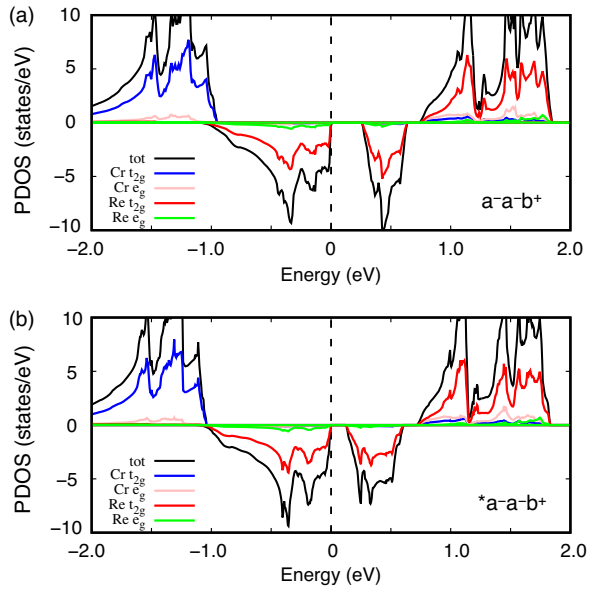

FIG. 16: DFT+U projected density of states of Ca_2CrReO_6 (a) in the ground state structure ($a^-a^-b^+$) (b) in the reference structure $*a^-a^-b^+$. The Fermi energy is set to be zero; $U_{\rm Re}$=2.0 and $U_{\rm Cr}$=2.5.

We now perform the same analysis as in the case of Ca_2FeReO_6, computing the orbital polarization, C-OD amplitude, band gap, and relative energy of the ground state structure $a^-a^-b^+$ and the reference structure $*a^-a^-b^+$ as a function of U (see Fig. 15). The same trends are observed as compared to Ca_2FeReO_6, with the only differences being quantitative changes due to the smaller effective Re bandwidth in the Cr-based systems. Interestingly, the C-OD amplitude rapidly saturates after its onset, and the relative energy difference ΔE shows three distinct regions. The third region, corresponding to $U_{\rm Re}$ >1.6 and $U_{\rm Cr}$=2.5, corresponds to the formation of the C-OO in the $*a^-a^-b^+$ reference structure, whereby the energy penalty of $U_{\rm Re}$ in the $*a^-a^-b^+$ structure is reduced via polarization. This region could not be clearly seen in the Ca_2FeReO_6 case given that the corresponding transition occurs just preceding the maximum value of $U_{\rm Re}$ in the plot, and the magnitude of the effect should be smaller given the larger effective Re bandwidth.

Most importantly, the critical threshold of $U_{\rm Re}$ for driving the MIT is strongly reduced, requiring only $U_{\rm Re}=1.4$ in the relaxed structure (with $U_{\rm Cr}=2.5$); and a similar renormalization occurs in the reference structure $*a^-a^-b^+$ which now only needs $U_{\rm Re}=1.7$ to achieve an insulating state. This has interesting implications, as the critical $U_{\rm Re}$ is now sufficiently small in the reference structure that the insulating state may survive in the absence of any appreciable C-OD amplitude. If we as-

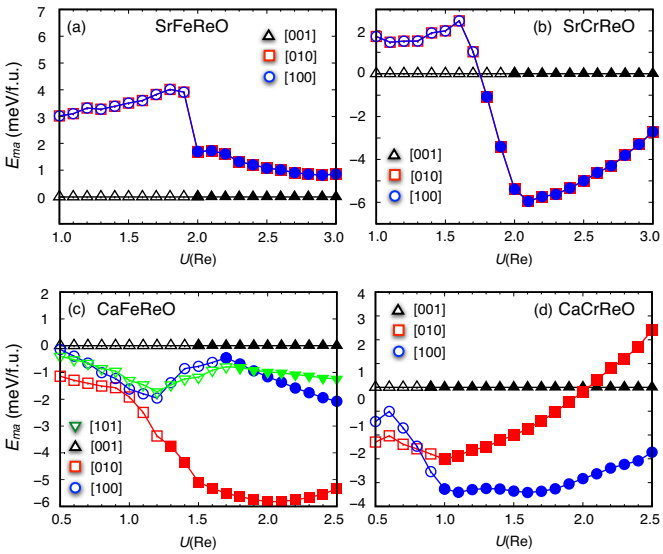

FIG. 17: Magnetic anisotropy energies as a function of $U_{\rm Re}$ for (a) Sr_2FeReO_6, (b) Sr_2CrReO_6, (c) Ca_2FeReO_6, and (d) Ca_2CrReO_6. Energies of the magnetization direction [001] (c-axis) is set to zero; $U_{\rm Fe}$=4 and $U_{\rm Cr}$=2.5. Empty and filled points stand for metallic and insulating phases, respectively.

sume our preferential values of $U_{\rm Re}=2$ and $U_{\rm Cr}=2.5$, we see that both the relaxed structure and the reference structure are insulators (see Fig. 16 for projected DOS). This result is consistent with the experimental measurements on Ca_2CrReO_6 which find no appreciable C-OD amplitude, as in our reference structure, yet still measure an insulating state[1,24]; though further experiments are clearly needed in this system before drawing conclusions.

One could argue that choosing a smaller value of $U_{\rm Re}$ could yield the same behavior as Ca_2FeReO_6, where the loss of the C-OD amplitude destroys the C-OO and results in an metallic state, but this sort of tuning would be forbidden by the fact that $U_{\rm Re}$ $\geq$2.0 is needed to obtain the experimentally observed insulating state in Sr_2CrReO_6. Therefore, Ca_2CrReO_6 could be a concise example where orbital ordering can clearly be observed in the (near) absence of a concomitant structural distortion (i.e. at a temperature where the C-OD is suppressed but the C-OO survives).

C. Effect of spin-orbit coupling

The strength of the spin-orbit coupling (λ) can be up to 0.5eV in the 5d transition metal oxides, which is non-negligible when compared to U and the bandwidth. In the better known example of the irridates, the t_{2g} bandwidth is approximately 1eV, and thus a spin-orbit coupling of λ=0.3-0.5eV plays an important role in realizing the insulating state[101–103]. The effect of SOC in the Re based DPs will be smaller than the irridates given that the t_{2g} bandwidth of Re is closer to 2eV and the strength of the SOC of Re will also be smaller due to the smaller atomic number of Re. For example, our comparison of the Re-projected DOS with and without SOC in the Sr-based systems demonstrated changes of approximately 0.2eV (see Fig. 3, panels c and d). While SOC does not qualitatively change any major trends, the small quantitative changes can be relevant; as we will demonstrate. In this section, we will explore the magnetic anisotropy energy as a function of $U_{\rm Re}$, in addition to repeating our previous analysis of the orbital polarization, the OD amplitude, band gap, and relative energetics. Here we will only consider $U_{\rm Fe}$=4 and $U_{\rm Cr}$=2.5.

We begin by considering the magnetic anisotropy energy (E_{ma}) as summarized in Fig. 17. We define E_{ma} as the relative energy (per Re) of a given magnetic orientation with respect to the energy of the [001] orientation (e.g. $E_{ma}[010] = E[010] - E[001]$). The magnetic orientation is particularly important since the threshold of $U_{\rm Re}$ for the C-OO/C-OD depends on the magnetic orientation, and shifts as large as 0.4eV can observed for Ca_2FeReO_6.

For Sr_2FeReO_6, the magnetization along [001] is most stable in our calculations, as shown in Fig 17 panel (a), whereas magnetic moments are aligned in ab-plane in the experiment at 298K[104]. This appears to be a discrepancy, though we only explored [100] and [010] directions within the ab-plane, so it is possible that some other direction within the plane is lower. Also, our calculations are at T=0, while the experiments were done at T=298K. Otherwise, this could serve as an interesting failure of the method (albeit for a very small energy scale). Nonetheless, Sr_2FeReO_6 is metallic with $U_{\rm Re}$ <2.0 in all orientations that we explored.

For Sr_2CrReO_6, the magnetization along the [100] and [010] directions are equivalent, as shown in Fig. 17 panel (b). Interestingly, [001] is more stable for small $U_{\rm Re}$, but then this trend is reversed once the system goes through the C-OO/C-OD and there is a magnetic easy ab plane for $U_{\rm Re}$ $\geq$1.8. Given our preferred values of $U_{\rm Re}$=1.9 and $U_{\rm Cr}$=2.5 (see Section III D), DFT+U results in an easy ab plane. Recent experiment by Lucy *et al.* showed that a Sr_2CrReO_6 film on $SrTiO_3$ and $(LaAlO_3)_{0.3}(Sr_2AlTaO_6)_{0.7}$, corresponding to 0.09% and 1.04% of compressive strains, results in a magnetic easy axis within the ab plane at both low (20K) and high T (300K)[105,106].

For Ca_2FeReO_6, Rietveld refinement determined that the magnetization easy axis below T_{MIT} is the b-axis (ie. [010]), while above T_{MIT} the magnetization easy axis changes[16,18]; though there is not yet consensus on the direction. Granado *et al.* suggested that Fe and Re moments lie on the ac-plane, where the magnetization angle from the a axis is 55° (close to [101])[18], whereas Oikawa *et al.* showed that [001] is the easy axis[16]. We will explore [100], [010], [001], and [101] in the ground state structure, while primarily focussing on [001] in the $*a^-a^-b^+$ reference structure; though with the latter we

investigate a few scenarios using [101].

By using the experimental atomic coordinates and LDA+U calculations ($U_{\rm Re}$=3 and $J_{\rm Re}$=0.7), Antonov *et al.* showed that [010] is the easy axis and [001] is lower in energy than [100], for both low T and high T experimental structures[23]. Gong *et al.* found the same result using the mBJ potential[107], despite the fact that they were using the GGA relaxed structure which more closely resembles the experimental structure above the phase transition. We also found the same ordering, which proved to be independent of the value of $U_{\rm Re}$, even when crossing the C-OO/C-OD transition (see Fig. 17, panel c). Given that above the MIT Granado *et al.* found [101] to be the easy-axis, we also explore this direction; demonstrating that it is very similar to [100]. Interestingly, the magnetic orientation can have an appreciable effect on the onset of C-OO/C-OD.

For Ca_2CrReO_6, we are not aware of any experimental data on the magnetic easy axis. From an mBJ study with GGA-relaxed structure, Gong *et al.* reported that [010] is the easy axis, and $E_{ma}[001] > E_{ma}[100]$[107]. Alternatively, our GGA+U+SOC calculations suggest that [100] is the easy axis for $U_{\rm Re} \geq 0.9$ (see Fig. 17, panel (d)). Given our preferred values of $U_{\rm Re}$=1.9 and $U_{\rm Cr}$=2.5 (see Section III D), we would expect an easy axis of [100] and that [010],[001] are very close in energy.

Having established the easy axis for each material, we now repeat the previous analysis probing the behavior as a function of the Hubbard U but now including SOC and the easy axis axis as determined from DFT+U (see Figs. 18-19); and it should be kept in mind that the predicted easy-axis for Sr_2FeReO_6 disagrees with experiment. Summarizing, we consider Sr_2FeReO_6 [001], Sr_2CrReO_6 [100], Ca_2FeReO_6 [010], and Ca_2CrReO_6 [100]. Given that SOC will break the block diagonal structure of the single-particle density matrix in the spin sector, it is useful to introduce a more general measure of orbital polarization rather than the definition used in equation (1); and we will utilize the standard deviation of the Eigenvalues of the local single particle density matrix for the correlated subspace, denoted σ_τ (this is a component of the DFT+U energy functional, see Ref.[108] for a detailed derivation):

$$\sigma_\tau = \sqrt{\frac{\sum_m (n^\tau_m - \mu_\tau)^2}{N_{\rm orb}}} \tag{2}$$

and

$$\mu_\tau = \frac{\sum_m n^\tau_m}{N_{\rm orb}} \ , \tag{3}$$

where m labels an Eigenvalue of the single-particle density matrix for the correlated subspace (ie. Eigenvalues of the 10×10 single-particle density matrix for the case of d electrons), τ labels a Re site in the unit cell, and $N_{\rm orb}$=10 for d-electrons. The orbital polarization is then defined to be σ_τ.

We begin with the Sr-based materials, Sr_2FeReO_6 and Sr_2CrReO_6, characterizing the effect of the SOC for the relaxed structure $a^0a^0c^-$+OD (e.g. $P4_2/m$ for $a^0a^0c^-$+C-OD, etc.) and the reference structure $I4/m$ ($*a^0a^0c^-$)(see Fig. 18). The previously presented results without SOC are included to facilitate comparison, in addition to providing updated values for our new metric of orbital polarization σ_τ. As expected, SOC is a relatively small perturbation in all cases, though there are some interesting differences. We begin by examining the orbital polarization for the reference structures $*a^0a^0c^-$ where the C-OD amplitude is restricted to be zero (see panels g and h). For smaller values of $U_{\rm Re}$, prior to the C-OO transition, SOC enhances the orbital polarization at a given value of $U_{\rm Re}$ in the F-OO state (comparing lines with up and down triangles). For Sr_2CrReO_6, the critical $U_{\rm Re}$ for the C-OO transition is shifted down by about 0.2eV (compare lines with up and down triangles), indicating the SOC is facilitating the onset of the C-OO and the resulting MIT. This renormalization of $U_{\rm Re}$ is much smaller for Sr_2FeReO_6 and cannot be seen at the resolution we have provided. In both cases, the magnitude of the orbital polarization beyond the C-OO transition is very similar with and without the SOC.

Allowing the C-OD to condense in the relaxed structures shows similar behavior (see red and blue curves). In both Sr_2FeReO_6 and Sr_2CrReO_6, SOC pushes the onset of the C-OO/C-OD to smaller values of $U_{\rm Re}$; more substantially in the case of Cr. As a result, including SOC causes the gap to open at slightly smaller values of $U_{\rm Re}$: approximately 0.1 less for Sr_2FeReO_6 and 0.2 less for Sr_2CrReO_6. Notably, the C-OD amplitude for the metallic phase of Sr_2FeReO_6 is dampened to zero, in agreement with experiment. Somewhat counterintuitively, SOC results in smaller C-OD amplitudes for values of $U_{\rm Re}$ beyond the MIT, despite causing an earlier onset of the C-OD. For the relative energetics, in both compounds SOC decreases the stabilization energy of the C-OD for $U_{\rm Re} \gtrapprox 2.1$ (see panels a and b), consistent with the reduced magnitude of the C-OD. Given our preferred value of $U_{\rm Re}$=1.9 for SOC, we find that Sr_2FeReO_6 is metallic with space group $I4/m$ (ie. no condensation of OD), consistent with experiment; while Sr_2CrReO_6 is insulating with a non-zero C-OD amplitude (i.e. space group $P4_2/m$), stabilized by roughly 14meV.

In the Ca-based systems, the effects of SOC are slightly more pronounced (see Fig. 19), which is likely associated with the smaller Re t_{2g} bandwidth, but the trends are all the same as the Sr-based materials. We begin by analyzing the orbital polarization in the reference structure $*a^-a^-b^+$, where the C-OD has effectively been removed (see panels g and h, curves with pink-up and blue-down triangles). For small values of $U_{\rm Re}$, SOC mildly enhances the orbital polarization, but the differences diminish once both cases form the C-OO insulator. However, SOC has a more dramatic effect in the Ca-based systems in terms of shifting the C-OO induced MIT to smaller values of $U_{\rm Re}$, giving a reduction of 0.7 and 0.4eV for the Fe-based

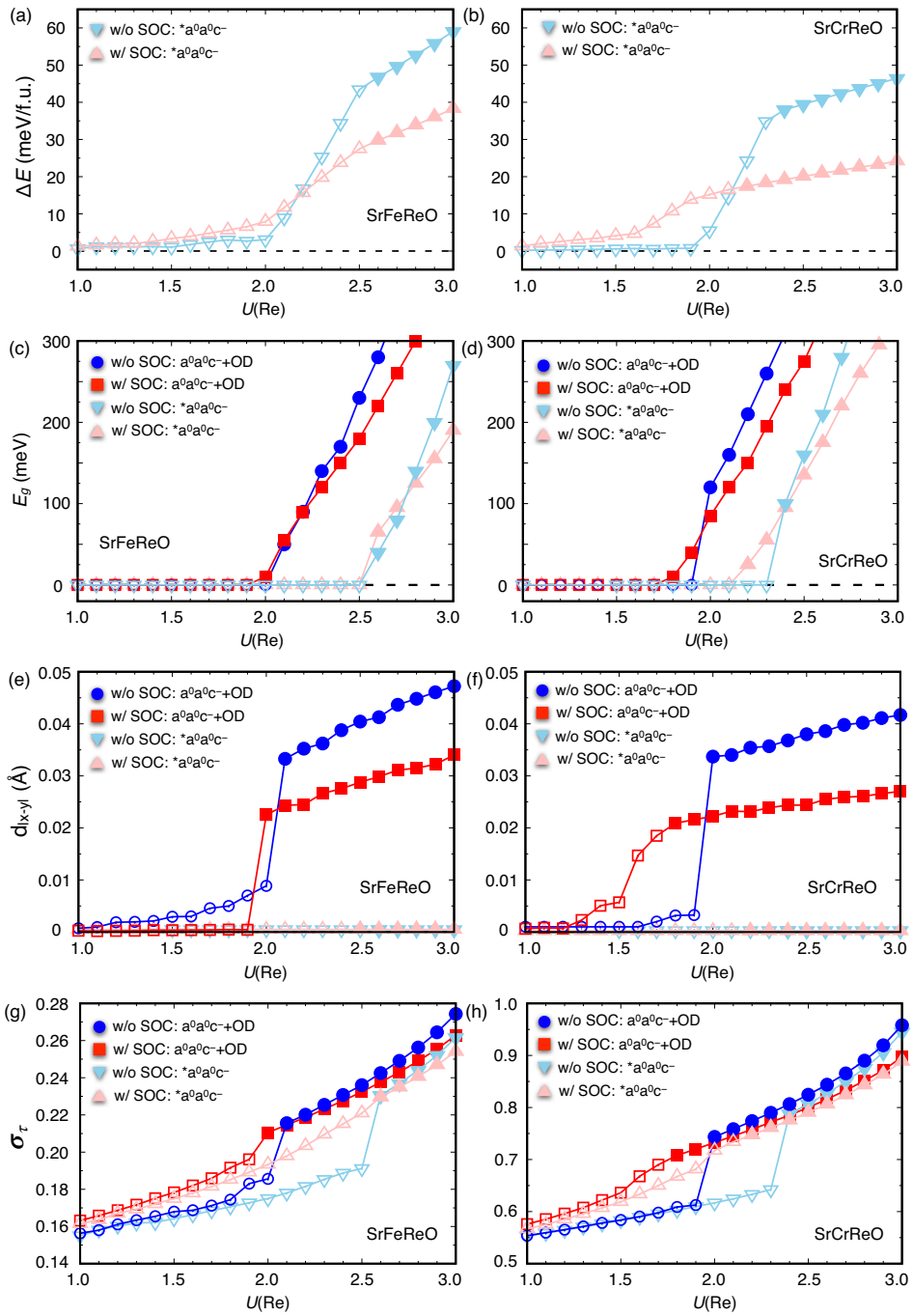

FIG. 18: (a),(b) Relative energy of Sr_2FeReO_6 and Sr_2CrReO_6 in the reference structure $I4/m$ with respect to the ground state (i.e. $a^0a^0c^-$+OD); with and without spin-orbit coupling. (c),(d) Electronic band gaps of different phases. (e),(f) Octahedral distortion (OD) amplitude $d_{|x-y|}$ of the ReO_6 octahedron. (g),(h) Orbital polarization σ_τ (see eq. 2) for Re. Panels (a), (c), (e), and (g) correspond to Sr_2FeReO_6 with $U_{\rm Fe}$=4, while panels (b), (d), (f), and (h) correspond to Sr_2CrReO_6 with $U_{\rm Cr}$=2.5. Filled and empty points stand for the insulating and metallic phases, respectively. Magnetization is along the [001] and [100] for Sr_2FeReO_6 and Sr_2CrReO_6, respectively.

and Cr-based material, respectively (see panels c and d, curves with pink-up and blue-down triangles). For the relaxed structures (see red and blue curves), the C-OD is activated at much smaller values of $U_{\rm Re}$ in both materials, more so for the case of Ca_2CrReO_6. Furthermore, Ca_2FeReO_6 reaches a relatively smaller value of the C-OD amplitude beyond the C-OO induced MIT, while Ca_2CrReO_6 saturates at roughly the same value. Given our preferred value of $U_{\rm Re}$=1.9, both Ca_2FeReO_6 and Ca_2CrReO_6 are insulators with a appreciable C-OD amplitude, consistent with known experiments (though the low temperature structural parameters of Ca_2CrReO_6 have not yet been measured). Furthermore, SOC has reduced the C-OD amplitude of Ca_2FeReO_6, moving it closer to the experimental value (see panel e, red curve).

For Ca_2FeReO_6, we also investigate the behavior of the [001] magnetization direction for both the reference structure $*a^-a^-b^+$ and the ground state structure $a^-a^-b^+$, which is essential given that experiment dictates [001] is approximately the easy-axis above the MIT where the C-OD is suppressed. For $a^-a^-b^+$, the [001] orientation is higher in energy than [010], with the difference

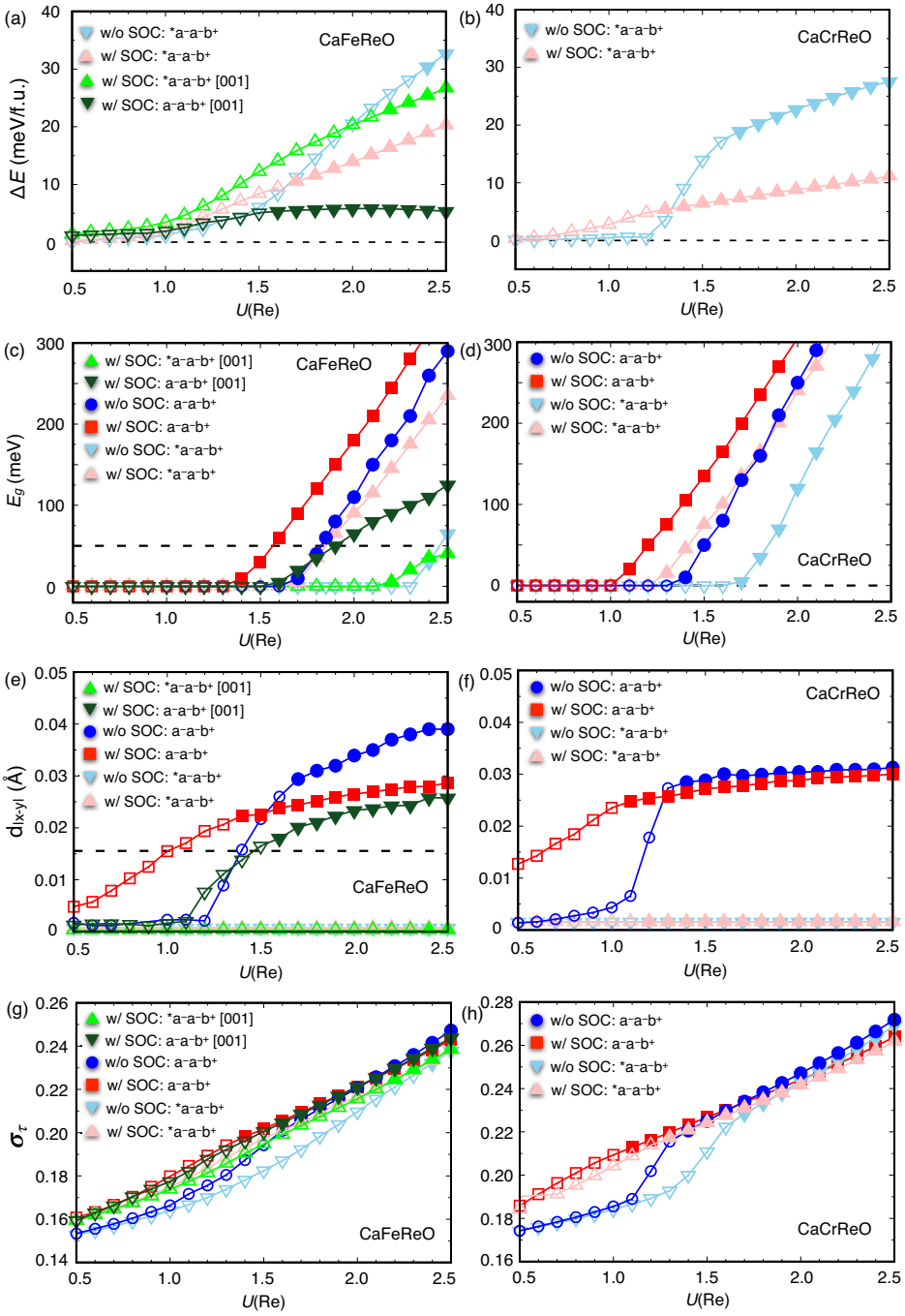

FIG. 19: (a),(b) Relative energy of Ca_2FeReO_6 and Ca_2CrReO_6 in the reference structure $*a^-a^-b^+$ with respect to the ground state (i.e. $a^-a^-b^+$); with and without spin-orbit coupling. (c),(d) Electronic band gaps of different phases. (e),(f) Octahedral distortion (OD) amplitude $d_{|x-y|}$ of the ReO_6 octahedron. (g),(h) Orbital polarization σ_τ (see eq. 2) for Re. Panels (a), (c), (e), and (g) correspond to Ca_2FeReO_6 with $U_{\rm Fe}$=4, while panels (b), (d), (f), and (h) correspond to Ca_2CrReO_6 with $U_{\rm Cr}$=2.5. Filled and empty points stand for the insulating and metallic phases, respectively. Magnetization is along the [010] and [100] for Ca_2FeReO_6 and Ca_2CrReO_6, respectively. Additionally, the [001] magnetization direction (experimentally observed for T]140K) is included for Ca_2FeReO_6 where indicated.

being enhanced as $U_{\rm Re}$ increases (see Fig. 17, panel c, green curve). Furthermore, for [001] the threshold value of $U_{\rm Re}$ for the onset of the C-OO/C-OD is increased, and the magnitude of the band gap and C-OD amplitude are diminished at a given value of $U_{\rm Re}$ (see Fig. 19, panels c and e, dark green triangles). More relevantly, the same trends are observed in the reference structure $*a^-a^-b^+$, but the effect is amplified (light green triangles). In particular, the critical value of $U_{\rm Re}$ for the C-OO/C-OD dramatically increases from 1.8 to 2.2 eV as the magnetization switches from [010] to [001] (compare pink and light green curves, respectively). We also investigate the case of [101] magnetization direction. The overall features of [101] are similar to the case of [001] (not shown), except that the critical value of $U_{\rm Re}$ for the C-OO/C-OD in the reference structure is increased to 2.4eV.

In Section III B 3, where SOC was not yet included, we elucidated the possibility that a suppression of the C-OD (e.g. via thermal fluctuations) closes the band gap via moving the critical value of $U_{\rm Re}$ beyond our expected value of $U_{\rm Re}$=2.0 within GGA+U (see Figure 14). This could have been a viable mechanism for the MIT, but SOC is strong enough to alter this scenario (see Figure 20, panels a and b, using $U_{\rm Re}$=1.9). Given the [010] magneti-

zation direction, the gap is reduced in the reference structure, but it does not close, unlike the case where SOC is not included. However, the experiments of Oikawa *et al.* dictate that [001] should be the easy axis of the high temperature structure, in contradiction with DFT+U+SOC using our reference structure (though our predicted energy difference is less than 6meV). If we consider the [001] direction in the reference structure $*a^-a^-b^+$, we see that the gap has indeed closed (see Figure 20, panel (c)); the gap also closes for the [101] direction. Therefore, it is possible that the reorientation of the magnetization is important to the MIT.

In summary, we see that for $U_{\rm Re}$=1.9, Sr_2FeReO_6 is a metal, while the remaining systems are C-OO induced insulators. The general physics that was deduced in the absence of SOC holds true with some small renormalizations of various observables. Slightly reducing the value of $U_{\rm Re}$ allows for results which are qualitatively consistent with experiment, with the caveat that the easy-axis of Sr_2FeReO_6 disagrees with experiment.

Another interesting feature of SOC is the nonzero orbital moments of Re. Spin and orbital moments of Re within GGA+SOC and GGA+U+SOC with $U_{\rm Re}$=1.9 are summarized in Table VII. The direction of Re orbital moment is opposite to the spin moment, in agreement with the previous experiments[25,109,110] and GGA+SOC[111,112].

As presented in Table VII, varying results have been measured for the magnitude of spin and orbital moments by different groups. However, the $|m_L/m_S|$ values are more or less consistent[25,109] since this quantity is not affected by possible uncertainties in the calculated number of holes[25], thus these values are better quantities to compare theory and experiments. While GGA largely underestimate the experimental $|m_L/m_S|$ values, GGA+U gives a much better estimation for $|m_L/m_S|$.

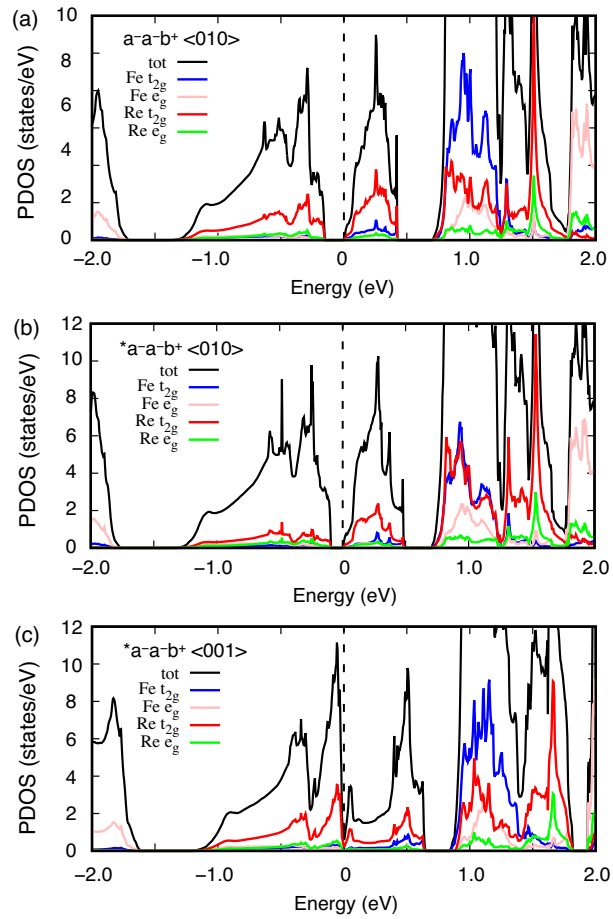

FIG. 20: DFT+U+SOC projected density of states of Ca_2FeReO_6 (a) in the ground state structure ($a^-a^-b^+$) with the [010] magnetization direction, (b) in the reference structure ($*a^-a^-b^+$) with the [010] magnetization direction, (c) in the reference structure ($*a^-a^-b^+$) with the [001] magnetization direction. The Fermi energy is set to be zero; $U_{\rm Re}$=1.9 and $U_{\rm Fe}$=4.

D. Optimal U values

Exploring a range of U is a necessary burden for several reasons. First, the procedure for constructing both the interactions and the double-counting correction is still an open problem. Second, given that the DFT+U method is equivalent to DFT+DMFT when the DMFT impurity problem is solved within Hartree-Fock[114], DFT+U contains well known errors which may be partially compensated by artificially renormalizing the U to smaller values. Given that our most basic concern in this paper is to develop a qualitative, and perhaps even semi-quantitative, understanding of an entire family of Re-based double perovskites, performing an empirical search for a single set of U's which can capture the physics of this family was essential.

In Sec III B and III C, we have explored various observables for a range of values of U. Clearly, $U_{\rm Re}$ is the main influence, as it is a necessary condition for driving the C-OO insulating state in the entire family of materials, in addition to the C-OD. However, we also demonstrated that the U of the 3d transition metal could play an important indirect role, via renormalizing the critical value of $U_{\rm Re}$ for the C-OO/C-OD to smaller values. Also, for the case of Sr_2CrReO_6, a nonzero $U_{\rm Cr}$ was important for properly capturing the energetics of the $a^0a^0c^-$ tilt pattern. For the 3d transition metals, we typically only explored U=0 and another value which is in line with expectations based on previous literature or methods for computing U. For Cr, we used $U_{\rm Cr}$=2.5 eV, which is similar to values used for $CaCrO_3$[115] and Cr-related DPs (U=3 eV and J=0.87 eV)[111]. For Fe, we focus on $U_{\rm Fe}$=4 eV, as widely used elsewhere[20,22,111]. Excessive tuning of $U_{\rm Fe}$ or $U_{\rm Cr}$ is not needed based on our results, and the nonzero values that we evaluated were either necessary to capture a given phenomena (i.e. the tilts in Sr_2CrReO_6), or were needed for a consistent and reasonable value of $U_{\rm Re}$ (via the indirect influence of the $U_{\rm Fe}$ or $U_{\rm Cr}$). There-

TABLE VII: Spin (m_S), orbital (m_L), and total (M_{tot}) moments of Re in DPs. Values are given in μ_B/Re.

	m_S	m_L	M_{tot}	$\lvert m_L/m_S \rvert$	method
Sr_2FeReO_6	−0.74	0.21	−0.53	0.28	exp[25]
	−1.07	0.33	−0.74	0.31	exp[109]
	−0.85	0.23	−0.62	0.27	GGA[111]
	−0.68	0.15	−0.53	0.22	GGA[25]
	−0.73	0.18	−0.55	0.25	LDA[23]
	−0.88	0.24	−0.64	0.28	LDA+U[23]
	−1.01	0.26	−0.75	0.26	mBJ[113]
	−0.76	0.16	−0.61	0.20	GGA
	−1.22	0.42	−0.83	0.34	GGA+U
Sr_2CrReO_6	−0.68	0.25	−0.43	0.37	exp[29]
	−0.85	0.18	−0.67	0.21	GGA[112]
	−1.17	0.31	−0.85	0.27	mBJ[113]
	−0.99	0.19	−0.80	0.19	GGA
	−1.40	0.48	−0.95	0.35	GGA+U
Ca_2FeReO_6	−0.47	0.16	−0.31	0.34	exp[25]
	−1.15	0.39	−0.76	0.34	exp[109]
	−0.75	0.34	−0.42	0.45	LDA[23]
	−1.11	0.66	−0.45	0.60	LDA+U[23]
	−1.10	0.18	−0.91	0.17	mBJ[107]
	−0.76	0.17	−0.58	0.23	GGA
	−1.30	0.43	−0.87	0.33	GGA+U
Ca_2CrReO_6	−1.24	0.19	−1.05	0.15	mBJ[107]
	−1.04	0.24	−0.80	0.23	GGA
	−1.41	0.56	−0.85	0.40	GGA+U

fore, $U_{\rm Fe}$=4 eV and $U_{\rm Cr}$=2.5 eV are reasonable values to adopt, though a range of values could likely give sufficient behavior.

In the case of $U_{\rm Re}$, we explored a large number of values between 0-3.2eV. The overall goal for selecting a set of U's is to obtain the proper ground states in the entire family of materials, which is nontrivial given that Sr_2FeReO_6 is metallic and the rest are insulators. While it is possible for $U_{\rm Re}$ to have small changes due to differences in screening among the four materials, these differences should be relatively small given the localized nature of the d orbitals which comprise the correlated subspace; and therefore we do seek a common value for all four compounds. We conclude that $U_{\rm Re}$=2.0 and 1.9 are reasonable values within GGA+U and GGA+U+SOC, respectively, and these values will properly result in a metal for Sr_2FeReO_6 and insulators for the rest. The predicted bandgap $E_{\rm gap}$ for Ca_2FeReO_6 (i.e. 105meV and 150meV within GGA+U and GGA+U+SOC, respectively) is somewhat larger than the experiment (i.e. 50meV), but this seems reasonable given the nature of approximations we are dealing with. For Ca_2CrReO_6, we obtain $E_{\rm gap}$=250 and 270meV using GGA+U and GGA+U+SOC, respectively (experimental gap is not known); while $E_{\rm gap}$ of Sr_2CrReO_6 within GGA+U and GGA+U+SOC is 120 and 40meV, respectively, somewhat smaller than the experimental value of 200meV[3].

It is also interesting to compute $U_{\rm Re}$ via the linear response approach[116]. In Sr_2CrReO_6 and Ca_2CrReO_6, we obtained $U_{\rm Re}$=1.3 for both systems; the calculation employed a supercell containing 8 Re atoms. Therefore, linear response predicts a relatively small value for U, consistent with 5d electrons, but too small in order to be qualitatively correct: Sr_2CrReO_6 could not be an insulator with such a small value.

E. Future challenges for experiment

The central prediction of our work is that the minority spin Re d_{xz}/d_{yz} orbitals order in a $\boldsymbol{q}_{\rm fcc} = \left(0, \frac{1}{2}, \frac{1}{2}\right)$ motif, along with occupied minority spin Re d_{xy} orbitals, in Sr_2CrReO_6, Ca_2FeReO_6, and Ca_2CrReO_6. This section explores how this prediction may be tested in experiment. This orbital ordering results in a narrow gap insulator in our calculations, consistent with the insulating states observed in experiment for these compounds (see Section I B). However, more direct signatures of the orbital ordering are desired.

Perhaps the most straightforward experiment is precisely resolving the crystal structure of insulating Sr_2CrReO_6 at low temperatures. Given that the C-OO breaks the symmetry of the $I4/m$ space group, inducing the C-OD, experiment may be able to detect the resulting $P4_2/m$ space group at low temperatures. Such a measurement would serve as a clear confirmation of our predicted orbital ordering.

Precisely resolving the bond lengths of Ca_2CrReO_6 at low temperatures would also be beneficial. While the C-OO/C-OD is not a spontaneously broken symmetry in Ca_2CrReO_6, an enhancement of $d_{|x-y|}$ is predicted in our calculations; similar to what has already been experimentally observed in the case of Ca_2FeReO_6.

Other experiments could possibly directly probe the orbital ordering, such as X-ray linear dichroism. Once again, Sr_2CrReO_6 may be the best test case given that the orbital ordering is a spontaneously broken symmetry.

IV. Summary

In summary, we investigate the electronic and structural properties of Re-based double perovskites A_2BReO$_6$ (A=Sr, Ca and B=Cr, Fe) through density-functional theory + U calculations, with and without spin-orbit coupling. All four compounds share a common low energy Hamiltonian, which is a relatively narrow Re t_{2g} minority spin band that results from strong antiferromagnetic coupling to filled 3d majority spin shell (or sub-shell) of the B ion. Cr results in a narrower Re t_{2g} bandwidth than Fe, while Ca-induced tilts result in a narrower Re t_{2g} bandwidth than Sr-induced tilts; resulting in a ranking of the Re t_{2g} bandwidth as Sr_2FeReO_6,

Sr_2CrReO_6, Ca_2FeReO_6, and Ca_2CrReO_6 (from largest to smallest). Spin orbit coupling is demonstrated to be a relatively small perturbation, though it still can result in relevant quantitative changes.

In general, we show that the on-site U_{Re} drives a C-type (i.e. $\boldsymbol{q}_{\mathrm{fcc}} = \left(0, \frac{1}{2}, \frac{1}{2}\right)$ given the primitive face-centered cubic unit cell of the double perovskite) antiferro orbital ordering (denoted C-OO) of the Re d_{xz}/d_{yz} minority spin orbitals, along with minority d_{xy} being filled on each site, resulting in an insulating ground state. This insulator is Slater-like, in the sense that the C-type ordering is critical to opening a band gap. Interestingly, this C-OO can even occur in a cubic reference structure ($Fm\bar{3}m$) in the absence of any structural distortions for reasonable values of U_{Re}. Furthermore, allowing structural distortions demonstrates that this C-OO is accompanied by a local E_g structural distortion of the octahedra with C-type ordering (denoted as C-OD); and it should be emphasized that U_{Re} is a necessary condition for the C-OO/C-OD to occur. The C-OO/C-OD will be a spontaneously broken symmetry for $a^0a^0c^-$-type tilt patterns as in the Sr based systems (i.e. $I4/m \rightarrow P4_2/m$), whereas not for the $a^-a^-b^+$-type tilting pattern of the Ca based systems (i.e. $P2_1/n \rightarrow P2_1/n$).

While U_{Re} is a necessary condition for obtaining an insulating state, the presence of the C-OD will reduce the critical value of U_{Re} necessary for driving the orbitally ordered insulating state; as will the U on the $3d$ transition metal. Furthermore, the C-OD is necessary for reducing the critical U_{Re} to a sufficiently small value such that Sr_2FeReO_6 remains metallic while Sr_2CrReO_6 is insulating. More specifically, using a single set of interaction parameters (i.e. $U_{\mathrm{Re}} = 1.9eV$, $U_{\mathrm{Fe}} = 4eV$, $U_{\mathrm{Cr}} = 2.5eV$, when using SOC), we show that Sr_2CrReO_6, Ca_2CrReO_6, and Ca_2FeReO_6 are all insulators, while Sr_2FeReO_6 is a metal; consistent with most recent experiments.

Previous experiments concluded that Sr_2CrReO_6 was half-metallic[1,2,24–26], but recent experiments showed that fully ordered films grown on an STO substrate are insulating[3,27]. We show that Sr_2CrReO_6 is indeed insulating with $U_{\mathrm{Re}} = 1.9eV$, so long as the structure is allowed to relax and condense the C-OD. Given that the C-OD is a spontaneously broken symmetry in this case, the challenge for experimental verification will be resolving the $P4_2/m$ space group at low temperatures instead of the higher symmetry $I4/m$ group.

While the C-OD is not a spontaneously broken symmetry in Ca_2FeReO_6, experiment dictates that there is an unusual discontinuous phase transition at T=140K between two structures with the same space group, $P2_1/n$; with the high temperature structure being metallic and the low temperature structure being insulating. The main structural difference between the experimental structures is the C-OD amplitude: $d_{|x-y|}$ is 0.016 and 0.005Å in the structures at 120K and 160K, respectively. Additionally, the C-OD changes variants across the transition, going from C-OD$^+$ (120K) to C-OD$^-$ (160K). The appreciable C-OD$^+$ amplitude measured in low temperature experiments is consistent with our prediction of a large C-OD amplitude which is induced by the C-OO. The same trends are found in Ca_2CrReO_6, which has a narrower Re bandwidth and results in a more robust insulator with a larger band gap. Predicting the transition temperature from first-principles will be a great future challenge given that the temperature of the electrons and the phonons may need to be treated on the same footing, all while accounting for the spin-orbit coupling.

SOC is a small quantitative effect, though it can have relevant impact, such as lowering the threshold value of U_{Re} for inducing the C-OO/C-OD in the Ca-based compounds; even having a strong dependence on magnetization direction for Ca_2FeReO_6. GGA+U+SOC predicts the easy axis of Sr_2CrReO_6 and Ca_2FeReO_6 to be {100} and [010], respectively, consistent with the experiment, and also compares well to the experimental measurements of the magnitude of the orbital moment. It should be emphasized that U_{Re}, and the C-OO/C-OD which it induces, is critical to obtaining the qualitatively correct easy-axis in Sr_2CrReO_6. In the case Sr_2FeReO_6, GGA+U+SOC predicts a [001] easy axis, in disagreement with one experiment which measured the easy axis to be in the $a-b$ plane. Additionally, the GGA+U+SOC predicted ratios of obital/spin moment m_L/m_s are close to the experimental values, whereas GGA+SOC largely underestimates them.

V. Acknowledgments

We thank to K. Oikawa and K. Park for helpful discussion. This work was supported by the grant DE-SC0016507 funded by the U.S. Department of Energy, Office of Science. This research used resources of the National Energy Research Scientific Computing Center, a DOE Office of Science User Facility supported by the Office of Science of the U.S. Department of Energy under Contract No. DE-AC02-05CH11231.

[1] H. Kato, T. Okuda, Y. Okimoto, Y. Tomioka, K. Oikawa, T. Kamiyama, and Y. Tokura, Phys. Rev. B **69**, 184412 (2004), URL `http://link.aps.org/doi/10.1103/PhysRevB.69.184412`.

[2] J. M. De Teresa, D. Serrate, C. Ritter, J. Blasco, M. R. Ibarra, L. Morellon, and W. Tokarz, Phys. Rev. B **71**, 092408 (2005), URL `http://link.aps.org/doi/10.1103/PhysRevB.71.092408`.

[3] A. J. Hauser, J. R. Soliz, M. Dixit, R. E. A. Williams, M. A. Susner, B. Peters, L. M. Mier, T. L. Gustafson,

M. D. Sumption, H. L. Fraser, et al., Phys. Rev. B **85**, 161201 (2012), URL http://link.aps.org/doi/10.1103/PhysRevB.85.161201.

[4] D. Serrate, J. M. D. Teresa, and M. R. Ibarra, Journal of Physics: Condensed Matter **19**, 023201 (2007), URL http://stacks.iop.org/0953-8984/19/i=2/a=023201.

[5] S. Vasala and M. Karppinen, Progress in Solid State Chemistry **43**, 1 (2015), ISSN 0079-6786, URL http://www.sciencedirect.com/science/article/pii/S0079678614000338.

[6] M. P. Singh, K. D. Truong, S. Jandl, and P. Fournier, Phys. Rev. B **79**, 224421 (2009), URL http://link.aps.org/doi/10.1103/PhysRevB.79.224421.

[7] J. B. Philipp, D. Reisinger, M. Schonecke, M. Opel, A. Marx, A. Erb, L. Alff, and R. Gross, Journal of Applied Physics **93**, 6853 (2003), URL http://scitation.aip.org/content/aip/journal/jap/93/10/10.1063/1.1556124.

[8] K. I. Kobayashi, T. Kimura, H. Sawada, K. Terakura, and Y. Tokura, Nature **395**, 677 (1998), URL http://dx.doi.org/10.1038/27167.

[9] H. Chen, A. J. Millis, and C. A. Marianetti, Phys. Rev. Lett. **111**, 116403 (2013), URL https://link.aps.org/doi/10.1103/PhysRevLett.111.116403.

[10] M. Karolak, M. Edelmann, and G. Sangiovanni, Phys. Rev. B **91**, 075108 (2015), URL https://link.aps.org/doi/10.1103/PhysRevB.91.075108.

[11] C. Kim, H. Park, and C. A. Marianetti, Phys. Rev. B **92**, 235122 (2015), URL https://link.aps.org/doi/10.1103/PhysRevB.92.235122.

[12] D. Puggioni, G. Giovannetti, M. Capone, and J. M. Rondinelli, Phys. Rev. Lett. **115**, 087202 (2015), URL https://link.aps.org/doi/10.1103/PhysRevLett.115.087202.

[13] N. Auth, G. Jakob, W. Westerburg, C. Ritter, I. Bonn, C. Felser, and W. Tremel, Journal of Magnetism and Magnetic Materials **272?276, Supplement**, E607 (2004), ISSN 0304-8853, proceedings of the International Conference on Magnetism (ICM 2003), URL http://www.sciencedirect.com/science/article/pii/S0304885303021772.

[14] J. M. De Teresa, D. Serrate, J. Blasco, M. R. Ibarra, and L. Morellon, Phys. Rev. B **69**, 144401 (2004), URL http://link.aps.org/doi/10.1103/PhysRevB.69.144401.

[15] H. Iwasawa, T. Saitoh, Y. Yamashita, D. Ishii, H. Kato, N. Hamada, Y. Tokura, and D. D. Sarma, Phys. Rev. B **71**, 075106 (2005), URL http://link.aps.org/doi/10.1103/PhysRevB.71.075106.

[16] K. Oikawa, T. Kamiyama, H. Kato, and Y. Tokura, Journal of the Physical Society of Japan **72**, 1411 (2003), http://dx.doi.org/10.1143/JPSJ.72.1411, URL http://dx.doi.org/10.1143/JPSJ.72.1411.

[17] B. Fisher, J. Genossar, K. Chashka, L. Patlagan, and G. Reisner, Journal of Magnetism and Magnetic Materials **316**, e713 (2007), ISSN 0304-8853, proceedings of the Joint European Magnetic Symposia, URL http://www.sciencedirect.com/science/article/pii/S0304885307004076.

[18] E. Granado, Q. Huang, J. W. Lynn, J. Gopalakrishnan, R. L. Greene, and K. Ramesha, Phys. Rev. B **66**, 064409 (2002), URL http://link.aps.org/doi/10.1103/PhysRevB.66.064409.

[19] W. Westerburg, O. Lang, C. Ritter, C. Felser, W. Tremel, and G. Jakob, Solid State Communications **122**, 201 (2002), ISSN 0038-1098, URL http://www.sciencedirect.com/science/article/pii/S0038109802000790.

[20] H. Wu, Phys. Rev. B **64**, 125126 (2001), URL http://link.aps.org/doi/10.1103/PhysRevB.64.125126.

[21] Z. Szotek, W. M. Temmerman, A. Svane, L. Petit, and H. Winter, Phys. Rev. B **68**, 104411 (2003), URL http://link.aps.org/doi/10.1103/PhysRevB.68.104411.

[22] B. C. Jeon, C. H. Kim, S. J. Moon, W. S. Choi, H. Jeong, Y. S. Lee, J. Yu, C. J. Won, J. H. Jung, N. Hur, et al., Journal of Physics: Condensed Matter **22**, 345602 (2010), URL http://stacks.iop.org/0953-8984/22/i=34/a=345602.

[23] V. N. Antonov, L. V. Bekenov, and A. Ernst, Phys. Rev. B **94**, 035122 (2016), URL http://link.aps.org/doi/10.1103/PhysRevB.94.035122.

[24] H. Kato, T. Okuda, Y. Okimoto, Y. Tomioka, Y. Takenoya, A. Ohkubo, M. Kawasaki, and Y. Tokura, Applied Physics Letters **81**, 328 (2002), http://dx.doi.org/10.1063/1.1493646, URL http://dx.doi.org/10.1063/1.1493646.

[25] A. Winkler, N. Narayanan, D. Mikhailova, K. G. Bramnik, H. Ehrenberg, H. Fuess, G. Vaitheeswaran, V. Kanchana, F. Wilhelm, A. Rogalev, et al., New Journal of Physics **11**, 073047 (2009), URL http://stacks.iop.org/1367-2630/11/i=7/a=073047.

[26] H. Asano, N. Kozuka, A. Tsuzuki, and M. Matsui, Applied Physics Letters **85**, 263 (2004), URL http://scitation.aip.org/content/aip/journal/apl/85/2/10.1063/1.1769085.

[27] A. J. Hauser, J. M. Lucy, H. L. Wang, J. R. Soliz, A. Holcomb, P. Morris, P. M. Woodward, and F. Y. Yang, Applied Physics Letters **102**, 032403 (2013), URL http://scitation.aip.org/content/aip/journal/apl/102/3/10.1063/1.4789505.

[28] J. M. Lucy, A. J. Hauser, H. L. Wang, J. R. Soliz, M. Dixit, R. E. A. Williams, A. Holcombe, P. Morris, H. L. Fraser, D. W. McComb, et al., Applied Physics Letters **103**, 042414 (2013), URL http://scitation.aip.org/content/aip/journal/apl/103/4/10.1063/1.4816803.

[29] P. Majewski, S. Geprgs, O. Sanganas, M. Opel, R. Gross, F. Wilhelm, A. Rogalev, and L. Alff, Applied Physics Letters **87**, 202503 (2005), URL http://scitation.aip.org/content/aip/journal/apl/87/20/10.1063/1.2131178.

[30] J. M. Michalik, J. M. D. Teresa, C. Ritter, J. Blasco, D. Serrate, M. R. Ibarra, C. Kapusta, J.Freudenberger, and N. Kozlova, EPL (Europhysics Letters) **78**, 17006 (2007), URL http://stacks.iop.org/0295-5075/78/i=1/a=17006.

[31] K. Kugel' and D. Khomskii, Journal of Experimental and Theoretical Physics **37**, 725 (1973), URL http://www.jetp.ac.ru/cgi-bin/e/index/e/37/4/p725?a=list.

[32] Y. Tokura and N. Nagaosa, Science **288**, 462 (2000).

[33] K. I. Kugel and D. I. Khomskii, Soviet Physics Uspekhi **25**, 231 (1982), URL http://stacks.iop.org/0038-5670/25/i=4/a=R03.

[34] J. Rodríguez-Carvajal, M. Hennion, F. Moussa, A. H. Moudden, L. Pinsard, and A. Revcolevschi, Phys. Rev. B **57**, R3189 (1998), URL https://link.aps.org/doi/10.1103/PhysRevB.57.R3189.

[35] P. Mandal, B. Bandyopadhyay, and B. Ghosh, Phys. Rev. B **64**, 180405 (2001), URL https://link.aps.org/doi/

10.1103/PhysRevB.64.180405.

[36] W.-G. Yin, D. Volja, and W. Ku, Phys. Rev. Lett. **96**, 116405 (2006), URL https://link.aps.org/doi/10.1103/PhysRevLett.96.116405.

[37] F. Moussa, M. Hennion, J. Rodriguez-Carvajal, H. Moudden, L. Pinsard, and A. Revcolevschi, Phys. Rev. B **54**, 15149 (1996), URL https://link.aps.org/doi/10.1103/PhysRevB.54.15149.

[38] M. C. Sánchez, G. Subías, J. García, and J. Blasco, Phys. Rev. Lett. **90**, 045503 (2003), URL https://link.aps.org/doi/10.1103/PhysRevLett.90.045503.

[39] L. G. Marshall, J. Zhou, J. Zhang, J. Han, S. C. Vogel, X. Yu, Y. Zhao, M. T. Fernández-Díaz, J. Cheng, and J. B. Goodenough, Phys. Rev. B **87**, 014109 (2013), URL https://link.aps.org/doi/10.1103/PhysRevB.87.014109.

[40] A. I. Liechtenstein, V. I. Anisimov, and J. Zaanen, Phys. Rev. B **52**, R5467 (1995), URL http://link.aps.org/doi/10.1103/PhysRevB.52.R5467.

[41] E. Pavarini, E. Koch, and A. I. Lichtenstein, Phys. Rev. Lett. **101**, 266405 (2008), URL https://link.aps.org/doi/10.1103/PhysRevLett.101.266405.

[42] I. Leonov, N. Binggeli, D. Korotin, V. I. Anisimov, N. Stojić, and D. Vollhardt, Phys. Rev. Lett. **101**, 096405 (2008), URL https://link.aps.org/doi/10.1103/PhysRevLett.101.096405.

[43] M. T. HUTCHINGS, E. J. SAMUELSEN, G. SHIRANE, and K. HIRAKAWA, Phys. Rev. **188**, 919 (1969), URL https://link.aps.org/doi/10.1103/PhysRev.188.919.

[44] L. Paolasini, R. Caciuffo, A. Sollier, P. Ghigna, and M. Altarelli, Phys. Rev. Lett. **88**, 106403 (2002), URL https://link.aps.org/doi/10.1103/PhysRevLett.88.106403.

[45] M. Cwik, T. Lorenz, J. Baier, R. Müller, G. André, F. Bourée, F. Lichtenberg, A. Freimuth, R. Schmitz, E. Müller-Hartmann, et al., Phys. Rev. B **68**, 060401 (2003), URL https://link.aps.org/doi/10.1103/PhysRevB.68.060401.

[46] B. Keimer, D. Casa, A. Ivanov, J. W. Lynn, M. v. Zimmermann, J. P. Hill, D. Gibbs, Y. Taguchi, and Y. Tokura, Phys. Rev. Lett. **85**, 3946 (2000), URL https://link.aps.org/doi/10.1103/PhysRevLett.85.3946.

[47] J. Hemberger, H.-A. K. von Nidda, V. Fritsch, J. Deisenhofer, S. Lobina, T. Rudolf, P. Lunkenheimer, F. Lichtenberg, A. Loidl, D. Bruns, et al., Phys. Rev. Lett. **91**, 066403 (2003), URL https://link.aps.org/doi/10.1103/PhysRevLett.91.066403.

[48] M. N. Iliev, A. P. Litvinchuk, M. V. Abrashev, V. N. Popov, J. Cmaidalka, B. Lorenz, and R. L. Meng, Phys. Rev. B **69**, 172301 (2004), URL https://link.aps.org/doi/10.1103/PhysRevB.69.172301.

[49] V. Fritsch, J. Hemberger, M. V. Eremin, H.-A. Krug von Nidda, F. Lichtenberg, R. Wehn, and A. Loidl, Phys. Rev. B **65**, 212405 (2002), URL https://link.aps.org/doi/10.1103/PhysRevB.65.212405.

[50] E. Pavarini, S. Biermann, A. Poteryaev, A. I. Lichtenstein, A. Georges, and O. K. Andersen, Phys. Rev. Lett. **92**, 176403 (2004), URL https://link.aps.org/doi/10.1103/PhysRevLett.92.176403.

[51] E. Pavarini, A. Yamasaki, J. Nuss, and O. K. Andersen, New Journal of Physics **7**, 188 (2005), URL http://stacks.iop.org/1367-2630/7/i=1/a=188.

[52] M. Mochizuki and M. Imada, Journal of the Physical Society of Japan **73**, 1833 (2004), http://dx.doi.org/10.1143/JPSJ.73.1833, URL http://dx.doi.org/10.1143/JPSJ.73.1833.

[53] M. Mochizuki and M. Imada, New Journal of Physics **6**, 154 (2004), URL http://stacks.iop.org/1367-2630/6/i=1/a=154.

[54] T. Arima, Y. Tokura, and J. B. Torrance, Phys. Rev. B **48**, 17006 (1993), URL https://link.aps.org/doi/10.1103/PhysRevB.48.17006.

[55] J.-G. Cheng, Y. Sui, J.-S. Zhou, J. B. Goodenough, and W. H. Su, Phys. Rev. Lett. **101**, 087205 (2008), URL https://link.aps.org/doi/10.1103/PhysRevLett.101.087205.

[56] A. C. Komarek, H. Roth, M. Cwik, W.-D. Stein, J. Baier, M. Kriener, F. Bourée, T. Lorenz, and M. Braden, Phys. Rev. B **75**, 224402 (2007), URL https://link.aps.org/doi/10.1103/PhysRevB.75.224402.

[57] L. J. P. Ament and G. Khaliullin, Phys. Rev. B **81**, 125118 (2010), URL https://link.aps.org/doi/10.1103/PhysRevB.81.125118.

[58] J. Akimitsu, H. Ichikawa, N. Eguchi, T. Miyano, M. Nishi, and K. Kakurai, Journal of the Physical Society of Japan **70**, 3475 (2001), http://dx.doi.org/10.1143/JPSJ.70.3475, URL http://dx.doi.org/10.1143/JPSJ.70.3475.

[59] M. Itoh, M. Tsuchiya, H. Tanaka, and K. Motoya, Journal of the Physical Society of Japan **68**, 2783 (1999), http://dx.doi.org/10.1143/JPSJ.68.2783, URL http://dx.doi.org/10.1143/JPSJ.68.2783.

[60] T. Kiyama, H. Saitoh, M. Itoh, K. Kodama, H. Ichikawa, and J. Akimitsu, Journal of the Physical Society of Japan **74**, 1123 (2005), http://dx.doi.org/10.1143/JPSJ.74.1123, URL http://dx.doi.org/10.1143/JPSJ.74.1123.

[61] F. Iga, M. Tsubota, M. Sawada, H. B. Huang, S. Kura, M. Takemura, K. Yaji, M. Nagira, A. Kimura, T. Jo, et al., Phys. Rev. Lett. **93**, 257207 (2004), URL https://link.aps.org/doi/10.1103/PhysRevLett.93.257207.

[62] H. Nakao, Y. Wakabayashi, T. Kiyama, Y. Murakami, M. v. Zimmermann, J. P. Hill, D. Gibbs, S. Ishihara, Y. Taguchi, and Y. Tokura, Phys. Rev. B **66**, 184419 (2002), URL https://link.aps.org/doi/10.1103/PhysRevB.66.184419.

[63] Y. Taguchi, Y. Tokura, T. Arima, and F. Inaba, Phys. Rev. B **48**, 511 (1993), URL https://link.aps.org/doi/10.1103/PhysRevB.48.511.

[64] Y. Okimoto, T. Katsufuji, Y. Okada, T. Arima, and Y. Tokura, Phys. Rev. B **51**, 9581 (1995), URL https://link.aps.org/doi/10.1103/PhysRevB.51.9581.

[65] P. Bordet, C. Chaillout, M. Marezio, Q. Huang, A. Santoro, S.-W. Cheong, H. Takagi, C. Oglesby, and B. Batlogg, Journal of Solid State Chemistry **106**, 253 (1993), ISSN 0022-4596, URL http://www.sciencedirect.com/science/article/pii/S0022459683712855.

[66] J.-S. Zhou, Y. Ren, J.-Q. Yan, J. F. Mitchell, and J. B. Goodenough, Phys. Rev. Lett. **100**, 046401 (2008), URL https://link.aps.org/doi/10.1103/PhysRevLett.100.046401.

[67] Y. Ren, A. A. Nugroho, A. A. Menovsky, J. Strempfer, U. Rütt, F. Iga, T. Takabatake, and C. W. Kimball, Phys. Rev. B **67**, 014107 (2003), URL https://link.aps.org/doi/10.1103/PhysRevB.67.014107.

[68] S. Miyasaka, T. Okuda, and Y. Tokura, Phys. Rev. Lett. **85**, 5388 (2000), URL https://link.aps.org/doi/10.1103/PhysRevLett.85.5388.

[69] S. Miyasaka, Y. Okimoto, M. Iwama, and Y. Tokura, Phys. Rev. B **68**, 100406 (2003), URL https://link.aps.org/doi/10.1103/PhysRevB.68.100406.

[70] M. De Raychaudhury, E. Pavarini, and O. K. Andersen, Phys. Rev. Lett. **99**, 126402 (2007), URL https://link.aps.org/doi/10.1103/PhysRevLett.99.126402.

[71] Z. Fang and N. Nagaosa, Phys. Rev. Lett. **93**, 176404 (2004), URL https://link.aps.org/doi/10.1103/PhysRevLett.93.176404.

[72] S. Miyasaka, Y. Okimoto, and Y. Tokura, Journal of the Physical Society of Japan **71**, 2086 (2002), https://doi.org/10.1143/JPSJ.71.2086, URL https://doi.org/10.1143/JPSJ.71.2086.

[73] M. Reehuis, C. Ulrich, P. Pattison, B. Ouladdiaf, M. C. Rheinstädter, M. Ohl, L. P. Regnault, M. Miyasaka, Y. Tokura, and B. Keimer, Phys. Rev. B **73**, 094440 (2006), URL https://link.aps.org/doi/10.1103/PhysRevB.73.094440.

[74] E. Benckiser, L. Fels, G. Ghiringhelli, M. Moretti Sala, T. Schmitt, J. Schlappa, V. N. Strocov, N. Mufti, G. R. Blake, A. A. Nugroho, et al., Phys. Rev. B **88**, 205115 (2013), URL https://link.aps.org/doi/10.1103/PhysRevB.88.205115.

[75] H. Kawano, H. Yoshizawa, and Y. Ueda, Journal of the Physical Society of Japan **63**, 2857 (1994), https://doi.org/10.1143/JPSJ.63.2857, URL https://doi.org/10.1143/JPSJ.63.2857.

[76] M. Noguchi, A. Nakazawa, S. Oka, T. Arima, Y. Wakabayashi, H. Nakao, and Y. Murakami, Phys. Rev. B **62**, R9271 (2000), URL https://link.aps.org/doi/10.1103/PhysRevB.62.R9271.

[77] G. R. Blake, T. T. M. Palstra, Y. Ren, A. A. Nugroho, and A. A. Menovsky, Phys. Rev. B **65**, 174112 (2002), URL https://link.aps.org/doi/10.1103/PhysRevB.65.174112.

[78] C. Ulrich, G. Khaliullin, J. Sirker, M. Reehuis, M. Ohl, S. Miyasaka, Y. Tokura, and B. Keimer, Phys. Rev. Lett. **91**, 257202 (2003), URL https://link.aps.org/doi/10.1103/PhysRevLett.91.257202.

[79] G. R. Blake, T. T. M. Palstra, Y. Ren, A. A. Nugroho, and A. A. Menovsky, Phys. Rev. Lett. **87**, 245501 (2001), URL https://link.aps.org/doi/10.1103/PhysRevLett.87.245501.

[80] E. Benckiser, R. Rckamp, T. Mller, T. Taetz, A. Mller, A. A. Nugroho, T. T. M. Palstra, G. S. Uhrig, and M. Grninger, New Journal of Physics **10**, 053027 (2008), URL http://stacks.iop.org/1367-2630/10/i=5/a=053027.

[81] A. S. Erickson, S. Misra, G. J. Miller, R. R. Gupta, Z. Schlesinger, W. A. Harrison, J. M. Kim, and I. R. Fisher, Phys. Rev. Lett. **99**, 016404 (2007), URL https://link.aps.org/doi/10.1103/PhysRevLett.99.016404.

[82] K. E. Stitzer, M. D. Smith, and H.-C. zur Loye, Solid State Sciences **4**, 311 (2002), ISSN 1293-2558, URL http://www.sciencedirect.com/science/article/pii/S1293255801012572.

[83] A. J. Steele, P. J. Baker, T. Lancaster, F. L. Pratt, I. Franke, S. Ghannadzadeh, P. A. Goddard, W. Hayes, D. Prabhakaran, and S. J. Blundell, Phys. Rev. B **84**, 144416 (2011), URL https://link.aps.org/doi/10.1103/PhysRevB.84.144416.

[84] H. J. Xiang and M.-H. Whangbo, Phys. Rev. B **75**, 052407 (2007), URL https://link.aps.org/doi/10.1103/PhysRevB.75.052407.

[85] G. Chen, R. Pereira, and L. Balents, Phys. Rev. B **82**, 174440 (2010), URL https://link.aps.org/doi/10.1103/PhysRevB.82.174440.

[86] J. Romhányi, L. Balents, and G. Jackeli, Phys. Rev. Lett. **118**, 217202 (2017), URL https://link.aps.org/doi/10.1103/PhysRevLett.118.217202.

[87] K.-W. Lee and W. E. Pickett, EPL (Europhysics Letters) **80**, 37008 (2007), URL http://stacks.iop.org/0295-5075/80/i=3/a=37008.

[88] S. Gangopadhyay and W. E. Pickett, Phys. Rev. B **91**, 045133 (2015), URL https://link.aps.org/doi/10.1103/PhysRevB.91.045133.

[89] S. Gangopadhyay and W. E. Pickett, Phys. Rev. B **93**, 155126 (2016), URL https://link.aps.org/doi/10.1103/PhysRevB.93.155126.

[90] D. Harada, M. Wakeshima, Y. Hinatsu, K. Ohoyama, and Y. Yamaguchi, Journal of Physics: Condensed Matter **12**, 3229 (2000), URL http://stacks.iop.org/0953-8984/12/i=14/a=302.

[91] S. Kanungo, K. Mogare, B. Yan, M. Reehuis, A. Hoser, C. Felser, and M. Jansen, Phys. Rev. B **93**, 245148 (2016), URL http://link.aps.org/doi/10.1103/PhysRevB.93.245148.

[92] J. L. Hyo-Shin Ahn, Do Duc Cuong and S. Han., Journal of the Korean Physical Society **49**, 1536 (2006), URL http://www.jkps.or.kr/journal/view.html?uid=8003&vmd=Full.

[93] J. He and C. Franchini, Phys. Rev. B **86**, 235117 (2012), URL https://link.aps.org/doi/10.1103/PhysRevB.86.235117.

[94] P. E. Blöchl, Phys. Rev. B **50**, 17953 (1994), URL http://link.aps.org/doi/10.1103/PhysRevB.50.17953.

[95] G. Kresse and D. Joubert, Phys. Rev. B **59**, 1758 (1999).

[96] G. Kresse and D. Joubert, Phys. Rev. B **59**, 1758 (1999), URL http://link.aps.org/doi/10.1103/PhysRevB.59.1758.

[97] J. P. Perdew, A. Ruzsinszky, G. I. Csonka, O. A. Vydrov, G. E. Scuseria, L. A. Constantin, X. Zhou, and K. Burke, Phys. Rev. Lett. **100**, 136406 (2008), URL http://link.aps.org/doi/10.1103/PhysRevLett.100.136406.

[98] H. Park, A. J. Millis, and C. A. Marianetti, Phys. Rev. B **92**, 035146 (2015), URL http://link.aps.org/doi/10.1103/PhysRevB.92.035146.

[99] J. Chen, A. J. Millis, and C. A. Marianetti, Phys. Rev. B **91**, 241111 (2015), URL http://link.aps.org/doi/10.1103/PhysRevB.91.241111.

[100] C. A. Marianetti, D. Morgan, and G. Ceder, Phys. Rev. B **63**, 224304 (2001).

[101] B. H. Kim, G. Khaliullin, and B. I. Min, Phys. Rev. Lett. **109**, 167205 (2012), URL https://link.aps.org/doi/10.1103/PhysRevLett.109.167205.

[102] H. Watanabe, T. Shirakawa, and S. Yunoki, Phys. Rev. Lett. **105**, 216410 (2010), URL https://link.aps.org/doi/10.1103/PhysRevLett.105.216410.

[103] B. J. Kim, H. Jin, S. J. Moon, J.-Y. Kim, B.-G. Park, C. S. Leem, J. Yu, T. W. Noh, C. Kim, S.-J. Oh, et al., Phys. Rev. Lett. **101**, 076402 (2008), URL https://link.aps.org/doi/10.1103/PhysRevLett.101.076402.

[104] S. Nakamura and K. Oikawa, Journal of the Physical Society of Japan **72**, 3123 (2003), http://dx.doi.org/10.1143/JPSJ.72.3123, URL http://dx.doi.org/10.1143/JPSJ.72.3123.

[105] J. M. Lucy, M. R. Ball, O. D. Restrepo, A. J. Hauser, J. R. Soliz, J. W. Freeland, P. M. Woodward, W. Windl, and

F. Y. Yang, Phys. Rev. B **90**, 180401 (2014), URL http://link.aps.org/doi/10.1103/PhysRevB.90.180401.

[106] J. M. Lucy, A. J. Hauser, Y. Liu, H. Zhou, Y. Choi, D. Haskel, S. G. E. te Velthuis, and F. Y. Yang, Phys. Rev. B **91**, 094413 (2015), URL https://link.aps.org/doi/10.1103/PhysRevB.91.094413.

[107] S. Gong, S.-D. Guo, P. Chen, and B.-G. Liu, RSC Adv. **5**, 63165 (2015), URL http://dx.doi.org/10.1039/C5RA09921H.

[108] E. B. Isaacs and C. A. Marianetti, Phys. Rev. B **95**, 045141 (2017).

[109] M. Sikora, C. Kapusta, M. Borowiec, C. J. Oates, V. Prochazka, D. Rybicki, D. Zajac, J. M. De Teresa, C. Marquina, and M. R. Ibarra, Applied Physics Letters **89**, 062509 (2006), URL http://scitation.aip.org/content/aip/journal/apl/89/6/10.1063/1.2234292.

[110] D. Serrate, J. M. D. Teresa, P. A. Algarabel, C. Marquina, J. Blasco, M. R. Ibarra, and J. Galibert, Journal of Physics: Condensed Matter **19**, 436226 (2007), URL http://stacks.iop.org/0953-8984/19/i=43/a=436226.

[111] H.-T. Jeng and G. Y. Guo, Phys. Rev. B **67**, 094438 (2003), URL http://link.aps.org/doi/10.1103/PhysRevB.67.094438.

[112] G. Vaitheeswaran, V. Kanchana, and A. Delin, Applied Physics Letters **86**, 032513 (2005), URL http://scitation.aip.org/content/aip/journal/apl/86/3/10.1063/1.1855418.

[113] S.-D. Guo, The European Physical Journal B **88**, 82 (2015), ISSN 1434-6036, URL http://dx.doi.org/10.1140/epjb/e2015-50883-1.

[114] G. Kotliar, S. Y. Savrasov, K. Haule, V. S. Oudovenko, O. Parcollet, and C. A. Marianetti, Rev. Mod. Phys. **78**, 865 (2006).

[115] A. C. Komarek, S. V. Streltsov, M. Isobe, T. Möller, M. Hoelzel, A. Senyshyn, D. Trots, M. T. Fernández-Díaz, T. Hansen, H. Gotou, et al., Phys. Rev. Lett. **101**, 167204 (2008), URL http://link.aps.org/doi/10.1103/PhysRevLett.101.167204.

[116] M. Cococcioni and S. de Gironcoli, Phys. Rev. B **71**, 035105 (2005), URL http://link.aps.org/doi/10.1103/PhysRevB.71.035105.